Remote Sensing of Environment 306 (2024) 114120

Contents lists available at ScienceDirect

Remote Sensing of Environment

journal homepage: www.elsevier.com/locate/rse

Quantifying decadal stability of lake reflectance and chlorophyll-*a* from medium-resolution ocean color sensors

Xiaohan Liu *, Mark Warren, Nick Selmes, Stefan G.H. Simis

Plymouth Marine Laboratory, Prospect Place, The Hoe, Plymouth PL1 3DH, United Kingdom

ARTICLE INFO

Edited by Menghua Wang

Keywords:
Chlorophyll-a
Remote sensing
Inland waters
MODIS-Aqua
MERIS
OLCI

ABSTRACT

Multi-decadal time-series of Lake Water-Leaving Reflectance (LWLR), part of the Lakes Essential Climate Variable, have typically been interrupted for the 2012–2016 period due to lack of an ocean color sensor with capabilities equivalent to MERIS (2002–2012) and OLCI (2016 - present). Here we assess, for the first time, the suitability of MODIS/Aqua to estimate LWLR and the derived concentration of chlorophyll-*a* (Chl*a*) at the global scale across optically complex water types, in an effort to fill these information gaps for climate studies. We first compare the normalized water-leaving reflectance (R_w) derived from two atmospheric correction algorithms (POLYMER and L2gen) against in situ observations. POLYMER shows superior performance, considering the agreement with in situ measurements and the number of valid outputs. An extensive assessment of nine Chl*a* algorithms is then performed on POLYMER-corrected R_w from MODIS observations. The algorithms are tested both in original parameterizations and following calibration against in situ measurements of Chl*a*. We find that the performance of algorithms parameterized per Optical Water Type (OWT) allows considerable improvement of the global Chl*a* retrieval capability. Using 3 years of overlapping observations between MODIS/Aqua and MERIS (2009–2011) and OLCI (2017–2019), respectively, MODIS-derived reflectance and Chl*a* products showed a reasonable degree of long-term stability in 48 inland water bodies. These water bodies, therefore, mark the candidates to study long-term environmental change.

1. Introduction

Inland water bodies constitute a critical global resource, serving as sources of drinking water, promoting tourism, ensuring food security, facilitating shipping, and harboring diverse aquatic habitats that are crucial to biodiversity and climate change resilience. These water bodies are highly vulnerable to environmental changes, responding swiftly to both atmospheric and landscape alterations (Adrian et al., 2009). Chemical and biological contamination as well as physical disturbance by human activities can further accelerate rates of change, leading to rapid decline in their economical, recreational, aesthetic, and ecological functions. Deterioration of inland water quality has garnered growing concern as a result of eutrophication and climate change (Bhagowati and Ahamad, 2019).

Lake color, or lake water-leaving reflectance (LWLR), was recognized by the Global Climate Observing System (GCOS) as an Essential Climate Variable in 2006 (https://gcos.wmo.int/en/essential-climate-variables/lakes/). LWLR can be used to relate changes in lake physics to biogeochemical properties, with the latter in water quality management context often being referred to as (optical) water quality. The requirements for observing LWLR combine extensive observation coverage and a high frequency of observations (at least weekly). Furthermore, to have relevance in climate studies, stability over multiple decades is also necessary. To meet these requirements at the global scale, remote sensing using a range of satellite platforms is clearly needed. Current efforts to realize such datasets are based on MERIS and OLCI for medium-resolution observation, providing global coverage of $<$3 days with a spatial resolution of $<$300 m (Attila et al., 2018; Donlon et al., 2012; Kratzer et al., 2008). These sensors leave an observation gap between the operation of MERIS (Apr 2002 - Apr 2012) and OLCI (Feb 2016 - now). Other sensors, such as Landsat, may extend observation time-series to prior decades, but do not meet requirements for temporal resolution, nor the diagnostic wavebands found on MERIS and OLCI to target specific biogeochemical substances at the required precision. Another operational ocean color sensor, the Moderate Resolution Imaging Spectroradiometer (MODIS) Aqua (2002 - present), has been collecting data with global coverage every 1–2 days at an equivalent spatial resolution (250/500/1000 m), showing promise in filling the

* Corresponding author.
E-mail address: liux@pml.ac.uk (X. Liu).

https://doi.org/10.1016/j.rse.2024.114120
Received 3 August 2023; Received in revised form 16 February 2024; Accepted 14 March 2024
Available online 23 March 2024

temporal observation gap. The waveband configuration of this sensor is, however, subtly different from MERIS and OLCI (Fig. 1), particularly regarding wavebands in the near-infrared which have proven important in observing optically complex inland and coastal waterbodies (Miller and McKee, 2004; Odermatt et al., 2012). To fulfill the Lakes Essential Climate Variable (ECV), it is a priority to consider the scope of applicability of MODIS-Aqua with a view to close the four-year observation gap.

Phytoplankton, forming the foundation of the aquatic food chain, plays a critical role in gauging alterations in the water environment that impact higher trophic levels. Consequently, phytoplankton abundance estimates offer insights into water quality and the functioning of aquatic ecosystems. Chlorophyll-*a* (Chl*a*) is the major photosynthetic pigment contained in phytoplankton and is widely used as a proxy for phytoplankton biomass (Kasprzak et al., 2008). The selective absorption of Chl*a* pigment causes a distinct spectral feature in water color that can be quantified from the water-leaving radiance measured in the visible portion of the electromagnetic radiation via optical remote sensing (Kirk, 2011; Mobley and Mobley, 1994).

Advances in optical remote sensing from the availability of multiple satellite sensors and retrieving algorithms have stimulated the Chl*a* remote sensing studies and led to development of both large-scale and long-term datasets for the purpose of ecosystem monitoring and climate research. Generating satellite Chl*a* time-series from multiple sensors has some challenges, including effective removal of atmospheric effects from at-sensor radiance signals and validation of satellite Chl*a* algorithms. MODIS-Aqua has shown radiometric drift in recent years, having already exceeded its initial design life, which is addressed through regular calibration and re-processing (Meister and Franz, 2014; Tilstone et al., 2013). Validation of the recalibrated MODIS-Aqua data and Chl*a* algorithms are subsequently required. Especially for inland waters, a high degree of optical diversity with varying complexity necessitates the validation and application of a range of algorithms, each applied within their design scope and subject to calibration against globally representative datasets (Neil et al., 2019). Although several MODIS Chl*a* algorithms have been validated in various lakes, these studies retain a regional scope or included relatively few candidate algorithms, and as such do not fully inform their suitability for global-scale application (Dall'Olmo et al., 2005; Gitelson et al., 2007; Ha et al., 2013; Qin et al., 2022; Zhang et al., 2016). Recently, an evaluation by Cao et al. (2022) assessed the performance of the MODIS surface reflectance product in monitoring global inland and coastal waters, indicating its potential to quantify parameters related to suspended particulate matter but facing challenges in Chl*a* retrieval. Previous studies evaluating MODIS and MERIS/OLCI water quality estimates were mostly performed regionally focusing on phytoplankton (e.g. cyanobacteria) bloom products (Qian et al., 2022; Wynne et al., 2021; Zeng and Binding, 2021). Therefore, there is still an obvious need to assess MODIS Chl*a* algorithms for inland waters, and generate the most accurate Chl*a* products possible to further enable a non-interrupted dataset for climate studies. In general, the accuracy of algorithms is contingent on their ability to account for variations in the bio-optical characteristics of water, subject to algorithm bands selection and goodness in trends simulations (Moses et al., 2009). Algorithms utilizing blue-green band ratios are expected to exhibit superior performance in waters with relatively low Chl*a* concentrations. However, they often yield lower accuracy than algorithms that employ NIR-red ratios in water with a high Chl*a* concentration, particularly in optically complex waters. This coincides with theoretical concerns that suggest the applicability of blue-green-based algorithms is restricted to open oceans where other optically active water constituents co-vary with Chl*a*. In turn, the performance of NIR-red algorithms is challenging in inland waters due to factors such as atmospheric mixing of light reflected from adjacent land, and the lower magnitude of water reflectance in the NIR-red region.

The primary objective of this study is to evaluate the performance of Chl*a* algorithms for MODIS over inland waters, and to ascertain their applicability within an Optical Water Type (OWT) classification framework which may circumvent some of the shortcomings in the design of MODIS with respect to MERIS and OLCI. We then identify lakes that could be integrated into a global dataset for seamless climatological studies. This, in turn, facilitates the creation of a continuous Chl*a* dataset for inland waters by providing a complementary approach to the methods delineated for OLCI and MERIS in Liu et al. (2021). In this study, (1) two atmospheric correction (AC) methods were compared on MODIS-Aqua data and validated using matchup in situ measurements; (2) nine Chl*a* algorithm candidates were evaluated, both in original and with recalibrated algorithm coefficients, and mapped against the OWT framework of 13 OWTs from inland water (Spyrakos et al., 2018); (3) inter-sensor stability between MERIS/OLCI and MODIS products was evaluated using concurrent satellite products during three years of overlap between MERIS and MODIS (2009–2011) and OLCI and MODIS (2017–2019), to inform the stability of the MODIS Chl*a* algorithm framework to a global set of water bodies, and identify potential lakes that could provide a relatively consistent data record over decades for climatological studies.

2. Data and methods

2.1. In situ and satellite data

2.1.1. In situ data

The validation dataset used in this study comprises 17 individual datasets from lakes and inland water bodies across the globe, requested through the LIMNADES repository (Lake Bio-optical Measurements and Matchup Data for Remote Sensing: http://www.limnades.stir.ac.uk). This combined data set consisted of 1982 individual observations of remote-sensing reflectance (R_{rs}, sr^{-1}) and 28,726 Chl*a* (mg/m^3) observations.

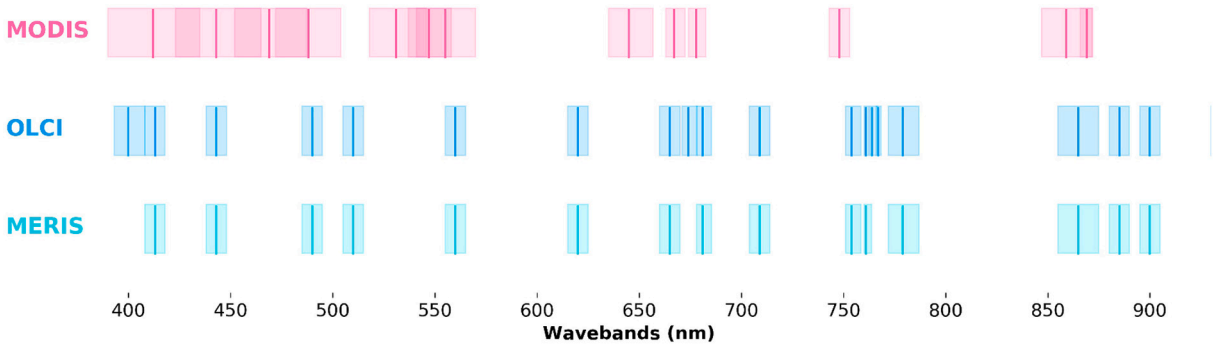

Fig. 1. Band configurations for MERIS, OLCI and MODIS.

2.1.2. Satellite data

Two AC approaches for MODIS were evaluated against in situ measurements: the L2gen and POLYMER algorithms. L2gen is the standard atmospheric correction algorithm used by the National Aeronautics and Space Administration Ocean Biology Processing Group, and this algorithm boasts extensive application on MODIS data, among other satellite sensors. It is designed to compensate for atmospheric effects that could adulterate satellite imagery. This encompasses adjustments for gaseous absorption, molecular scattering, and aerosol extinction in the Top of Atmosphere radiance measurements, alongside efficient cloud detection and evasion. The POLYMER algorithm is particularly known for its ability to handle sun glint, which could significantly enhance spatial coverage in comparison to other algorithms that falter under such challenging conditions. Its application extends across multiple sensors including MODIS, offering a robust multi-sensor atmospheric correction capability. This feature can be important for projects that aim to combine or compare data from different satellite sensors.

The current version of L2gen uses radiative transfer simulations and precomputed ancillary information to resolve the AC in an iterative process (Bailey et al., 2010). POLYMER v4.13 (Steinmetz et al., 2011) is the AC processor for lake water-leaving reflectance used in the ESA Lakes_cci (the ESA Climate Change Initiative for lakes) and the Copernicus Land Monitoring Service, resulting from previous round-robin comparisons of six AC algorithms for MERIS, including MEGS8.1 (MERIS standard), FUB, CoastColour, Case2Regional, SCAPE-M, and POLYMER, as detailed in Simis et al. (2020). This algorithm is based on spectral optimization using the whole spectral range from blue to NIR bands and has the ability to work in sun glint affected areas. MODIS L1A data were obtained from NASA for the period of 2002–2019 and processed to L1C using SeaDAS (v7.5.3). The Idepix classification tool (SNAP toolbox) was used to identify water pixels, to which both the POLYMER and L2gen were applied. For both AC algorithms, R_w data excluded from the analysis were those classified by L1B and Idepix flags as cosmetic, duplicated, glint risk, suspect, land, bright, coastline, and L1_invalid from the L1B product flag set, and cloud, cloud ambiguous, cloud sure, cloud buffer, cloud shadow, snow/ice, white and (mixed) land from Idepix. The resulting normalized water-leaving reflectance (R_w) was then compared to in situ remote-sensing reflectance, R_{rs}, assuming $R_w = R_{rs} \times \pi$.

MODIS satellite extractions were obtained as the median value of all valid pixels within 3 × 3 pixels around the location of the in situ measurements in satellite images collected within a ± 1-day window of the measurement time. This resulted in 937 and 243 matchups between in situ and MODIS observations for Chl*a* and R_{rs}, respectively. Fig. 2a shows the global distribution of the matchups. The matchup values of Chl*a*, R_{rs} at 488 and 667 nm were approximately normally distributed in log space (Fig. 2b), with respective median ± standard deviations of 22.0 ± 25.3 mg/m^3, 0.015 ± 0.013 sr^{-1}, and 0.015 ± 0.01 sr^{-1}, respectively.

To quantify the stability between observations from MODIS, MERIS, and OLCI, daily L3 products for 2009 to 2011 (MERIS) and 2017 to 2019 (OLCI) were obtained from the Lakes_cci v2.0.2 dataset, providing a 3-year overlap with MODIS. The L3 data are the result of nearest-neighbour reprojection to a global 1/120 degree grid (approximately 1 km) with a daily aggregation interval obtained by averaging the available input products.

For each lake and each sensor combination, the daily median values of valid observations for R_w and Chl*a* were extracted for the stability quantification. A total of 48 lakes were shown in this study which were previously selected from 1100 evaluated lakes. Specifically, two variables were selected for the evaluation including one water quality parameter (Chl*a*) and one water-leaving reflectance band (POLYMER corrected R_w at 488/490 nm). It is noted that 488 nm is a MODIS band, and 490 nm is the corresponding MERIS/OLCI band. For brevity, R_w(488) was used to refer to this band for the three sensors thereafter. For all of the 1100 evaluated lakes, three statistical analyses were conducted on extracted daily median values of the two variables (Chl*a* and R_w(488)): two-sided *t*-test, linear regression analysis and Kendall's Tau (τ) value. Lakes with $p > 0.001$ (from *t*-test), correlation coefficient (R) > 0.5 and $\tau > 0.5$ were selected which finally resulted in 48 lakes, covering a range of sizes from 121 to 83,961 km^2 and optical-biogeochemical properties (ultra-oligotrophic to eutrophic) across Europe, Africa, Asia, Oceania, and North and South America (Fig. 2 and Table 1).

Time-series and spatial variations of R_w and Chl*a* for the three sensors are further detailed for Lake Sevan (Armenia), which is the largest high-mountain lake in the Caucasus region and a major strategic resource for drinking water. The lake is known to have undergone eutrophication status shifts in the last few decades, mainly influenced by manually regulated lake water level fluctuations and environmental changes (Gevorgyan et al., 2020). The detailed observations of Lake Sevan serve to further evaluate and demonstrate the capability of Chl*a*

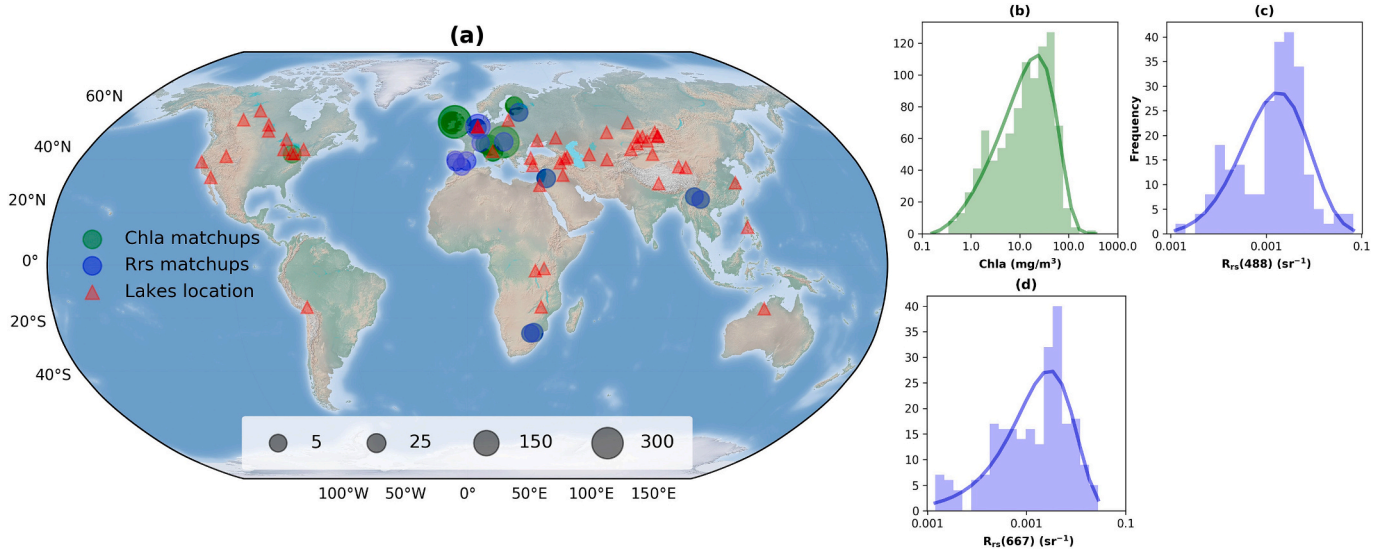

Fig. 2. (a) In situ matchup locations, and frequency distribution of (b) chlorophyll-*a* concentration, (c) R_{rs} at 488 nm, and (d) R_{rs} at 667 nm. Red triangles indicate the location of the 48 lakes in the stability quantification between MERIS, OLCI and MODIS. (For interpretation of the references to color in this figure legend, the reader is referred to the web version of this article.)

Table 1
Description of lakes included in the stability evaluations between MERIS, OLCI, and MODIS.

	Lake name	Continents	Area (km^2)	Trophic Status and optical characteristics*	Latitude	Longitude
1	Superior	North America	83,961	Ultra-oligotrophic, clear lake with low Chl*a* and total suspended matter (TSM) concentration	47.71	−87.75
2	Victoria	Africa	67,006	Mesotrophic lake with varying water clarity across its expanse, moderate high Chl*a* and TSM concentration	−1.27	32.87
3	Michigan	North America	58,257	Historically ultra-oligotrophic and had clear waters, which has experienced a decline in water clarity in recent decades	43.85	−87.08
4	Erie	North America	25,938	Mesotrophic. The western basin is eutrophic, often experiences reduced clarity due to sediment resuspension and algal blooms, while the eastern basin generally has clearer waters	42.14	−81.24
5	Ontario	North America	19,842	Oligotrophic, generally has clear water	43.83	−77.63
6	Titicaca	South America	7753	Mesotrophic, generally clear, some regions can be influenced by sediment resuspension or algal growth	−15.92	−69.30
7	Athabasca	North America	7691	Mesotrophic, whose clarity can fluctuate, especially with sediment inputs from rivers, particularly during spring runoff	59.11	−109.88
8	Great Salt	North America	5048	Eutrophic, one of the saltiest bodies of water in the world, often turbid due to sediment re-suspension	41.18	−112.59
9	Manitoba	North America	4792	Eutrophic, high Chl*a*, seasonal phytoplankton blooms could present	51.00	−98.79
10	Zaysan	Asia	4334	Eutrophic, high Chl*a*, seasonal phytoplankton blooms could present	48.72	83.43
11	Qinghai	Asia	4250	Oligotrophic, clear salt water	36.89	100.05
12	Sarykamyshskoye	Asia	3853	Oligotrophic, drainless saltwater lake, clear water	41.96	57.36
13	Uvs	Asia;Europe	3630	Oligotrophic, saline lake, clear water	50.34	92.76
14	Van	Asia	3594	Oligotrophic, saline lake, clear water	38.66	42.81
15	Alakol	Asia	2970	Oligotrophic, saline water, sediments flowing in from rivers and streams.	46.12	81.68
16	Kivu	Africa	2731	Mesotrophic, mostly clear	−2.04	29.16
17	Cedar	North America	2653	Eutrophic, seasonal phytoplankton blooms could present	53.33	−100.33
18	Cabora Bassa	Africa	2504	Mesotrophic, moderate-high Chl*a*	−15.72	32.04
19	Tsimlyanskoye	Europe	2445	Eutrophic, artificial lake, high Chl*a*	48.32	43.18
20	Tai	Asia	2416	Eutrophic, highly productive turbid shallow lake	31.24	120.14
21	Kakhovskoye	Europe	2149	Eutrophic, water reservoir	47.26	33.95
22	Buhayrat ath Tharthar	Asia	1629	Ultra-oligotrophic, very low Chl*a*, shoreline occasionally subjected to dust storms.	34.04	43.20
23	Curonian	Europe	1565	Hypertrophic, high Chl*a*, with cyanobacteria blooms	55.31	21.15
24	Khyargas	Asia	1400	Oligotrophic, salt lake	49.15	93.45
25	Qapshaghay Bogeni	Asia	1279	Mesotrophic, moderate-high Chl*a*	43.83	77.64
26	Sevan	Asia	1246	Mesotrophic, experiencing cyanobacteria blooms in recent years	40.39	45.35
27	Saint Clair	North America	1235	Mesotrophic, moderate-high Chl*a*	42.49	−82.70
28	Tengiz	Asia	1226	Eutrophic, shallow lake, high Chl*a*, subject to seasonal variations in water level	50.45	68.91
29	Bosten	Asia	1162	Mesotrophic, moderate high Chl*a* and TSM	41.98	87.06
30	Lesser Slave	North America	1146	Eutrophic, high Chl*a*, cyanobacteria blooms observed in west basin	55.41	−115.06
31	Ijsselmeer	Europe	1139	Eutrophic, high Chl*a*	52.81	5.37
32	Novosibirskoye	Europe	1136	Eutrophic, an artifical lake	54.30	81.78
33	Zhari Namco	Asia	985	Oligotrophic, salt lake, clear water	30.91	85.61
34	Salton	North America	961	Hypertrophic, salt lake, very high Chl*a*	33.31	−115.78
35	Argyle	Oceania	900	Mesotrophic, moderate-high Chl*a*	−16.36	128.67
36	Laguna de Bay	Asia	889	Eutrophic, productive water, turbid in dry season	14.36	121.14
37	Ulungar	Asia	865	Mesotrophic, moderate-high Chl*a*	47.22	87.21
38	Markermeer	Europe	717	Eutrophic, shallow lake, turbid and productive	52.51	5.25
39	Markakol	Asia	456	Mesotrophic, low total suspended matter	48.74	85.74
40	Mingechaurskoye	Asia	439	Mesotrophic, moderate-high Chl*a*	40.92	46.75
41	Iznik	Asia	303	Mesotrophic, moderate-high Chl*a*	40.44	29.53
42	Great Bitter	Africa	218	Mesotrophic, shallow salt lake, high Chl*a*	30.30	32.39
43	Airag	Asia	181	Eutrophic, high Chl*a*	48.89	93.44
44	Tudakul	Asia	162	Mesotrophic, moderate-high Chl*a*	39.85	64.84
45	Clear	North America	159	Eutrophic, high Chl*a*	39.03	−122.78
46	Burdur	Asia	158	Eutrophic, high Chl*a*	37.73	30.17
47	Toson	Asia	137	Oligotrophic, low Chl*a*	37.15	96.94
48	Trasimeno	Europe	121	Eutrophic, high Chl*a* and TSM, subject to the occurrence of seasonal algal blooms	43.14	12.10

* The trophic state was estimated from the lake average MODIS Chl*a* products according to Carlson and Simpson (1996).

products from multiple satellite sensors to describe long-term hydrological and environmental changes.

2.2. Algorithms

At present, the majority of published inland water quality algorithms are tailored to MERIS and OLCI sensors (Neil et al., 2019). In our research, we selected nine Chl*a* algorithms, encompassing a comprehensive range of empirical or semi-analytical algorithms previously published for the MODIS waveband set (Fig. 1). A round-robin comparison was performed to assess the MODIS algorithms for Chl*a*. The algorithms under comparison included three blue-green band ratio algorithms, three NIR-red band ratio algorithms, one peak height algorithm, and two semi-analytical algorithms (Table 2).

Table 2
Summary of validated chlorophyll-*a* models tested for MODIS.

Model	Architectural approach	Bands	Original training range (mg. m^{-3})	Reference
OC3	Blue-green ratio	*min* [443, 488], 547	0.012–77	https://oceancolor.gsfc.nasa.gov/atbd/chlor_a/
OC2	Blue-green ratio	488, 547	0.012–77	https://oceancolor.gsfc.nasa.gov/atbd/chlor_a/
OC2_HI	Blue-green ratio	469, 555	0.012–77	https://oceancolor.gsfc.nasa.gov/atbd/chlor_a/
R748_667	NIR-red ratio	748, (667 or 678)	4–240	Dall'Olmo et al. (2005); Gitelson (1992); Gitelson et al. (2008); Gitelson et al. (2007); Gurlin et al. (2011)
Shi	NIR-red ratio	645, 859	6.6–113.7	Shi et al. (2015)
Appel	NIR-red ratio	645, 859, 469	2.9–91	El-Alem et al. (2012)
FLH	Peak height	665, 677, 746	1–10	Letelier and Abbott (1996)
QAA_v6	Semi-analytical	\	0–70	https://www.ioccg.org/groups/Software_OCA/QAA_v6_2014209.pdf
GSM	Semi-analytical	\	0.02–10	Maritorena et al. (2002)

2.3. Optical water type framework

Spyrakos et al. (2018) used a gap statistic (Tibshirani et al., 2001) technique to select 13 distinct OWTs corresponding to specific combinations of bio-optical characteristics and the spectral shape of hyperspectral in situ reflectance. This analysis was against the same database (LIMNADES) as used in this study. Whilst from the same source, the in situ Chl*a* observations used in this study form a different subset from the earlier work because the coincidence of Chl*a* and MODIS observations is used to make the present selection.

To define the similarity between observed and reference OWT spectra, the spectral angle (Kruse et al., 1993) is used. This method emphasizes differences in spectral shape between the OWTs and reduces the influence of reflectance amplitude, making it a good choice for optically diverse inland waters (Liu et al., 2021). The spectral angle between an observed and reference spectrum is calculated as:

$$\alpha = cos^{-1}\frac{\sum_{i=1}^{n} p_i r_i}{\sqrt{\sum_{i=1}^{n} p_i^2}\sqrt{\sum_{i=1}^{n} r_i^2}} \quad (1)$$

$$S_{OWT} = 1 - \alpha/\pi \quad (2)$$

Where p_i is the per-pixel reflectance in band i for the observed spectrum and r_i is the reference spectrum reflectance in band i, and α is the spectral angle between the observed and reference spectrum, measured in radians. The result of the similarity test is a membership score for each of the 13 reference OWTs. The score (S_{OWT}) ranges from 0 to 1, where 1 implies identically shaped spectra. Fig. 3 summarizes the distribution of in situ Chl*a* grouped by the dominant OWT (the OWT with the highest S_{OWT}). More samples (>70 per OWT) were primarily associated with OWTs 2, 3, 6, 8, and 9, while fewer samples (<10 per OWT) were most similar to OWTs 1, 5, and 13. OWT 3 was associated with the widest Chl*a* range and the largest number of samples. OWTs 4, 6, 8, and 11 show the highest Chl*a* concentrations, with mean values >30 mg/m^3.

The assessed Chl*a* algorithms are finely tuned for each OWT by utilizing the matchups with the top 40% of membership scores for each OWT, and the best-performing mapping of algorithm and OWT is adopted in the OWT framework. Weighted-averaging of the Chl*a* algorithms using normalized S_{OWT} weights provides the blended Chl*a* product. Because some algorithm-OWT combinations are assumed to be non-physical, have low sensitivity, or may even deteriorate the blended result, only the top three S_{OWT} weights are considered. The remaining S_{OWT} weights are normalized by scaling them between one for the highest S_{OWT} and zero for the 4th ranking S_{OWT}.

2.4. Time-series trend detection

By combining MERIS, MODIS, and OLCI retrieved Chl*a* products,

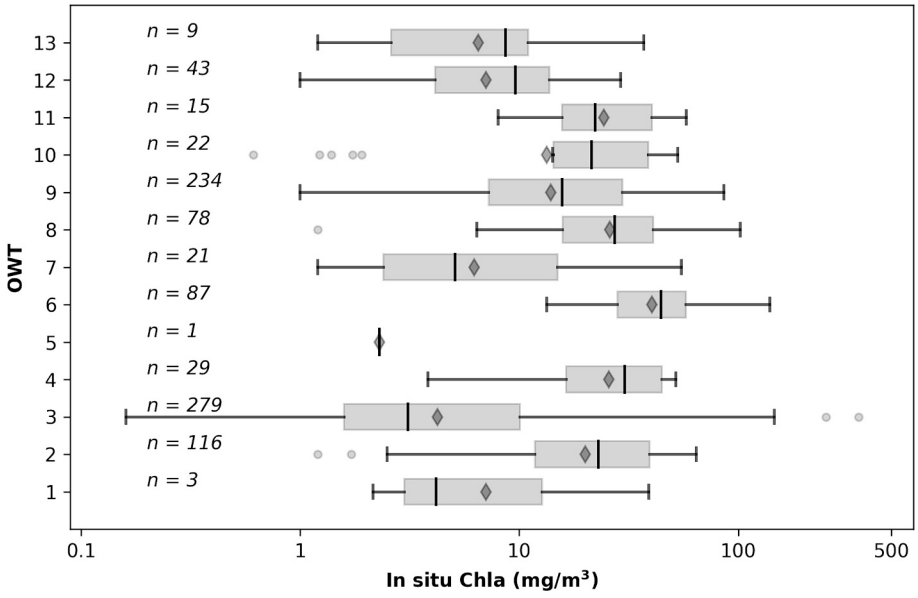

Fig. 3. Boxplots of in situ chlorophyll-*a* concentration for each OWT. The main body of the boxplot shows the 25th and 75th percentiles; the median and mean values are shown as vertical lines and diamonds, respectively.

uninterrupted satellite observation of phytoplankton can be achieved. As a demonstration of the application of the continuous Chl*a* product, daily median of lake water level (LWL) and lake water surface temperature (LWST) in Lake Sevan were extracted from the Lakes_cci v2.0.2 dataset from 2002 to 2020, which incorporates the Chl*a* product generation method outlined in the present work. The MERIS and OLCI Chl*a* products in this dataset are also the result of OWT-based blending, although the algorithm assignment and optimization were performed as described in previous work (Liu et al., 2021; Neil et al., 2019). To capture the inter-annual variability of Chl*a* and relative environmental variables (i.e., LWL and LWST), the time-series of monthly averaged data was calculated from daily products and subsequently deseasonalized by applying the 'seasonal_decompose' filter in the statsmodels.tsa package using Python v3.7.

2.5. Performance evaluation

Chl*a* algorithms were evaluated in three forms: a) original form (ORG), which adopts the proposed original parameterization of the model coefficients from literature, b) calibrated form (CAL), where model coefficients were tuned using the entire in situ dataset, c) clustered form (CLUS), where coefficients were fitted using subsets of the dataset corresponding to the highest similarity scores for each OWT. For the latter selections, coincident satellite and in situ observations where S_{OWT} was in the highest 40% were included.

A scoring system was applied to select the most appropriate algorithm for each OWT, following the scheme described in Neil et al. (2019). Eight statistical metrics were included in the evaluation: root mean square error (RMSE), mean absolute error (MAE), mean absolute percentage error (MAPE), bias, fraction of valid outputs, as well as the correlation coefficient, slope, and intercept from linear regression analysis. A further scoring system was applied whereby the median value for each error metric was compared between algorithms. One point was assigned for error statistics around the median of the statistic for all algorithms, while zero or two points were awarded when the metric was statistically better or worse than the median statistic, respectively. The scores of the eight metrics were then summed for each algorithm to provide a performance ranking with high scores corresponding to better-performing algorithms. The error metrics were produced on log10-transformed Chl*a* to give an approximately normal distribution, and to reduce the influence of high observation values on the statical metric results.

The RMSE, Normalized Root Mean Square Error (NRMSE), MAE, MAPE, and Bias were calculated as follows:

$$RMSE = \sqrt{\frac{1}{n}\sum_{i=1}^{n}(x_{re} - x_{is})^2} \tag{3}$$

$$NRMSE = \frac{\sqrt{\frac{1}{n}\sum_{i=1}^{n}(x_{re} - x_{is})^2}}{\frac{1}{n}\sum_{i=1}^{n}x_{is}} \bullet 100\% \tag{4}$$

$$MAE = \frac{1}{N}\sum_{i=1}^{N}|x_{re} - x_{is}| \tag{5}$$

$$MAPE = \frac{1}{N}\sum_{i=1}^{N}\frac{|x_{re} - x_{is}|}{x_{is}} \bullet 100\% \tag{6}$$

$$Bias = x_{re} - x_{is} \tag{7}$$

Where x_{re} is the retrieved value from algorithms, and x_{is} is the value of in situ observations. In addition, the Unbiased Mean Absolute Percentage difference (UMAP) is introduced specifically for R_w validation:

$$UMAP = \frac{1}{n}\sum_{i=1}^{n}\frac{|UD_i|}{x_{is}} \tag{8}$$

Where the Unbiased Difference (UD) is defined as the difference between the satellite R_w and the linear regression fit between all in situ and satellite R_w matchups. This is introduced to remove systematic effects from the atmospheric-corrected R_w, which can be eliminated by individual calibration on the downstream Chl*a* algorithms (Liu et al., 2021).

3. Results

3.1. Match-up validation of water-leaving reflectance

The performance of POLYMER and L2gen on MODIS R_w matchups was assessed at nine wavebands from 443 nm to 748 nm (Fig. 4), with linear regression statistics shown in Table 3. Significant linear correlations were found for all bands between in situ and satellite R_w atmospherically-corrected from both algorithms, with the highest $R = 0.83$ returned at 547 nm for POLYMER and $R = 0.85$ returned at 555 nm for L2gen (Fig. 4 and Table 3). Systematic underestimation was observed for both POLYMER and L2gen AC compared to the in situ observations. The POLYMER-corrected R_w showed UMAPE ranging from 28.1% at 547 nm to 61.7% at 678 nm, and bias ranging from −0.073 at 555 nm to −0.018 at 443 nm (Fig. 4 and Table 3). The L2gen correction showed UMAPE ranging from 33.9% at 555 nm to 139.6% at 443 nm, and bias ranging from −0.0157 at 748 nm to −0.0839 at 555 nm. Taking all evaluated bands and statistics into account, POLYMER-corrections showed better performance than L2gen with a significantly higher number of valid matchups resulting (243 vs 139). Therefore, POLYMER was adopted for further analyses.

3.2. Round-robin comparison of Chla algorithms

Fig. 5 shows round-robin comparison results of Chl*a* generated from each of the examined algorithms against the in situ measurements. Corresponding error metrics are shown in.

Fig. 6. OCX, R748_667, and QAA algorithms demonstrate a combined capability to estimate Chl*a* across the concentration range. Notably, algorithms OC2 and OC3 produced R values of 0.66 and NRMS of ~40% compared to in situ measurements. Algorithms Shi, Appel, and FLH performed poorly over the observed concentration range. The apparent failures that occur with algorithms Shi and Appel may be related to their usage of $R_w(859)$, which is not used in other algorithms, and leads to negative estimates of the calculated index. The FLH algorithm exhibits limited sensitivity across the full spectrum of Chl*a* concentrations, even after tuning. This finding is consistent with a study which suggests that this algorithm is effective exclusively in waters with low Chl*a* concentrations (i.e., <1 mg/m^3) when used with MODIS (Zhao et al., 2022). Among the three model forms, the per-cluster optimized algorithms ('Clus') provide the most accurate estimation of Chl*a*. It is noted that the GSM model is a semi-analytical inversion model with the application of a nonlinear least square optimization routine, for which no re-calibration was performed.

3.3. OWT-specific algorithm performance and assignment

Algorithm performance within subsets of the dataset corresponding to individual OWTs (data points within the highest 40% S_{OWT}) identified the OC2, OC3, OC2_HI algorithms (O'Reilly et al., 1998), and R748_667 algorithm (Dall'Olmo et al., 2005) as best performers across four sets of OWTs (Table 4 and Fig. 7). There were no valid performance scores for OWT 5, considering that only 1 sample was identified as dominant by it (Fig. 3). Within each OWT group, the selected algorithm was specifically tuned for each OWT. The resulting algorithm coefficients are provided in Appendix A (Table A1).

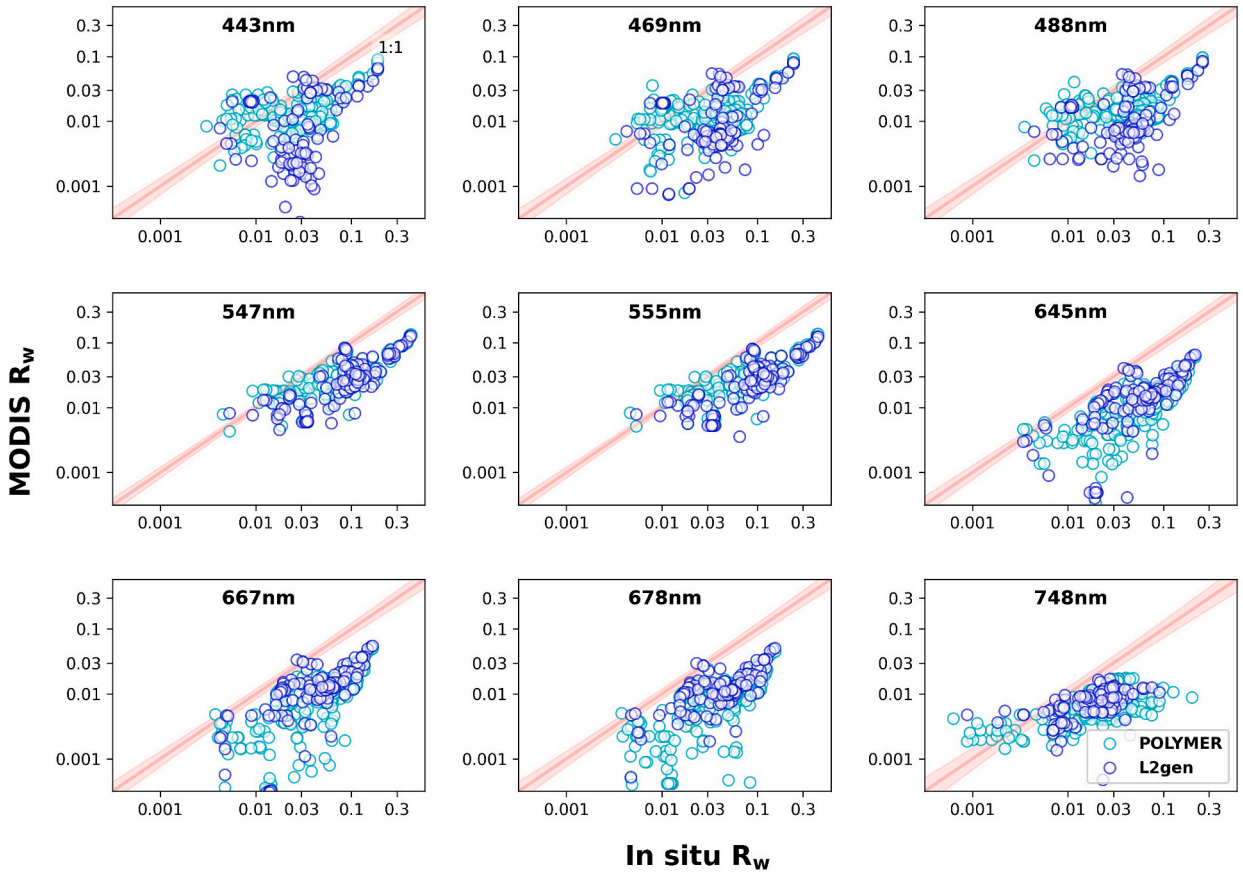

Fig. 4. POLYMER and L2gen matchups of MODIS with in situ reflectance data from LIMNADES: utilizing a ± 1-day matchup window and 3 × 3 pixel extraction window, presented in logarithmic coordinates.

Table 3
Descriptive statistics of the validation for matchups between in situ measurements and MODIS reflectance atmospheric-corrected by POLYMER and L2gen, respectively.

Processor	POLYMER (N = 243)				L2gen (N = 139)			
Wavebands	R	RMSE	UMAPE (%)	Bias	R	RMSE	UMAPE (%)	Bias
443	0.72	0.0285	46.6	−0.0179	0.54	0.0407	139.6	−0.0281
469	0.76	0.0407	50.5	−0.0286	0.65	0.0496	131.9	−0.0347
488	0.76	0.0452	39.4	−0.0315	0.71	0.0552	105.1	−0.0397
547	0.83	0.0914	28.1	−0.0703	0.84	0.1020	34.0	−0.0790
555	0.82	0.0948	30.5	−0.0733	0.85	0.1080	33.9	−0.0839
645	0.77	0.0614	59.3	−0.0502	0.78	0.0607	42.8	−0.0488
667	0.76	0.0477	50.1	−0.0387	0.77	0.0461	43.7	−0.0370
678	0.73	0.0453	61.7	−0.0370	0.77	0.0430	45.2	−0.0348
748	0.40	0.0297	34.8	−0.0207	0.33	0.0207	37.6	−0.0157
Average	0.73	0.0538	44.6	−0.0409	0.69	0.0584	68.2	−0.0446

3.4. *Weighted-blending algorithms in an optical water type framework*

The final Chl*a* product is the result of the weighted-blending procedure described in Section 2.3, with weights determined by the per-pixel OWT membership scores. The comparison between in situ and final Chl*a* product is shown in Fig. 8, giving an R value of 0.67 and NRMS of 43%.

3.5. *Inter-sensor comparison with MERIS and OLCI observations*

3.5.1. *Cross-sensor validation of water-leaving reflectance and Chla*

Cross-sensor validation between MERIS, OLCI, and MODIS for R_w and Chl*a* in 48 lakes shows generally good agreement (Fig. 9 and Table 5). The best stability between MODIS and MERIS is found at band 555 nm with R = 0.92, slope = 0.98, RMSE = 0.0119, MAPE = 13.2%, and bias = 0.0019, respectively. The correlation coefficient between MODIS and MERIS ranged from 0.80 at 748 nm to 0.92 at 555 nm, with relatively high MAPE >30% found in near-infrared bands. Similar evaluation results can be found between MODIS and OLCI, with band 555 nm showing the best stability. The regression line has a slope of 1, with an R = 0.92 and MAPE = 9.3% (Fig. 9d and Table 5). The correlation between Chl*a* derived with MODIS and MERIS or OLCI shows good linear relationships (Fig. 9h). On average, MODIS and OLCI show slightly better stability than MODIS and MERIS.

To enhance understanding of inter-sensor stability in relation to OWTs, satellite matchups from all studied lakes were grouped according to the OWT with the highest similarity. Table 6 shows the statistical correlation between satellites at 555–560 nm, grouped by OWT. The

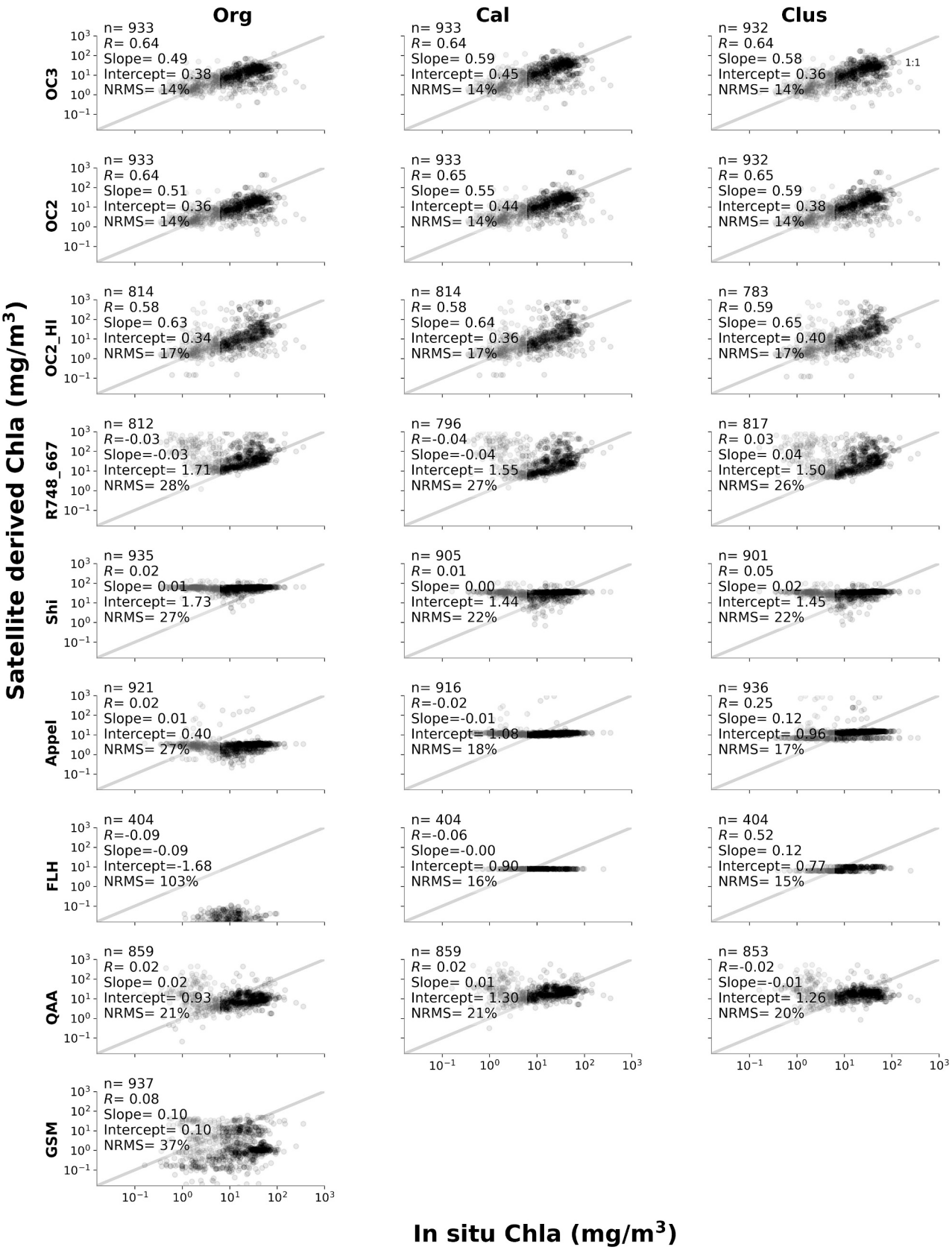

Fig. 5. Comparison of in situ measured and algorithm retrieved chlorophyll-*a* concentration for MODIS with the original algorithm definition in the first column, calibration against the whole dataset in the second column, and per-cluster optimized algorithms in the third column. Black line marks unity.

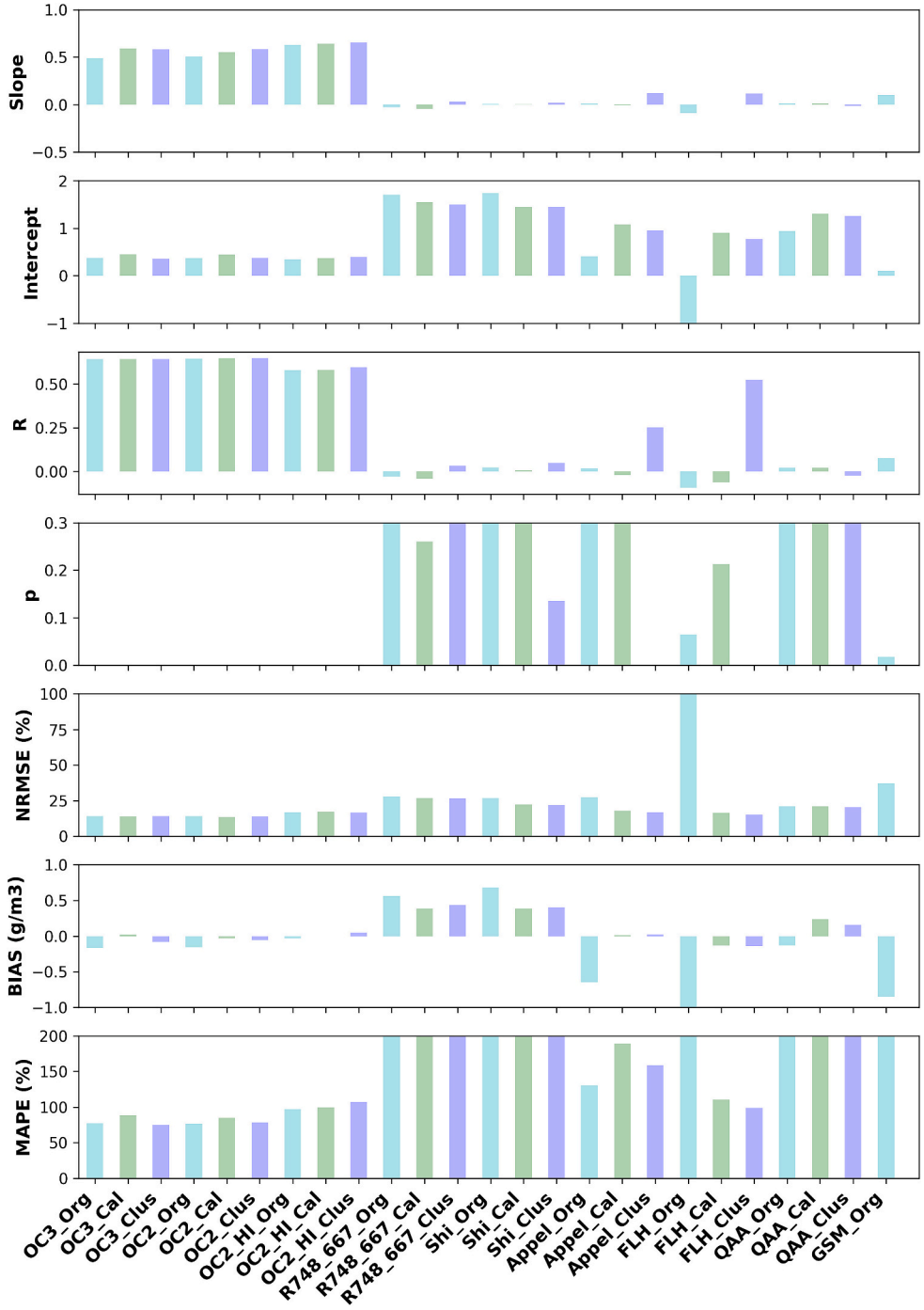

Fig. 6. Statistical metrics calculated between MODIS-derived and in situ chlorophyll-*a* concentration.

Table 4
Chlorophyll-*a* algorithms per optical water type for MODIS.

Product	Algorithm	Optical Water Type number
Chl*a*	OC2 oceancolor.gsfc.nasa.gov/cms/atbd/chlor_a	1, 5, 7, 9, 12,13
	OC3 oceancolor.gsfc.nasa.gov/cms/atbd/chlor_a	2, 3, 8
	R748/667 empirical band ratio based on Dall'Olmo et al. (2005)	4, 6, 11
	OC2_HI oceancolor.gsfc.nasa.gov/cms/atbd/chlor_a	10

majority of matchups corresponded most strongly to OWTs 3, 9, and 2. OWT 3 marks relatively clear water, while OWTs 9 and 2 exhibit a balanced influence of Chl*a*, CDOM, and inorganic suspended solids.

MODIS and OLCI demonstrated better agreement than MODIS and MERIS, indicated by genrerally higher correlation coefficients and slope values closer to 1. OWTs with a higher matchup frequency, such as OWTs 3, 9, 2, 4, 6, and 11, exhibited more consistent inter-sensor stability. To demonstrate the potential impact of MODIS band saturation, the 'return rate' of MODIS (N_return) was calculated, which quantifies the percentage of successful MODIS observations in comparison with corresponding MERIS or OLCI data collected on the same day. It is found that the N_return are above ~55% for most OWTs. However, a slightly lower incidence of N_return was observed for OWTs 5, 7 and 10 for both

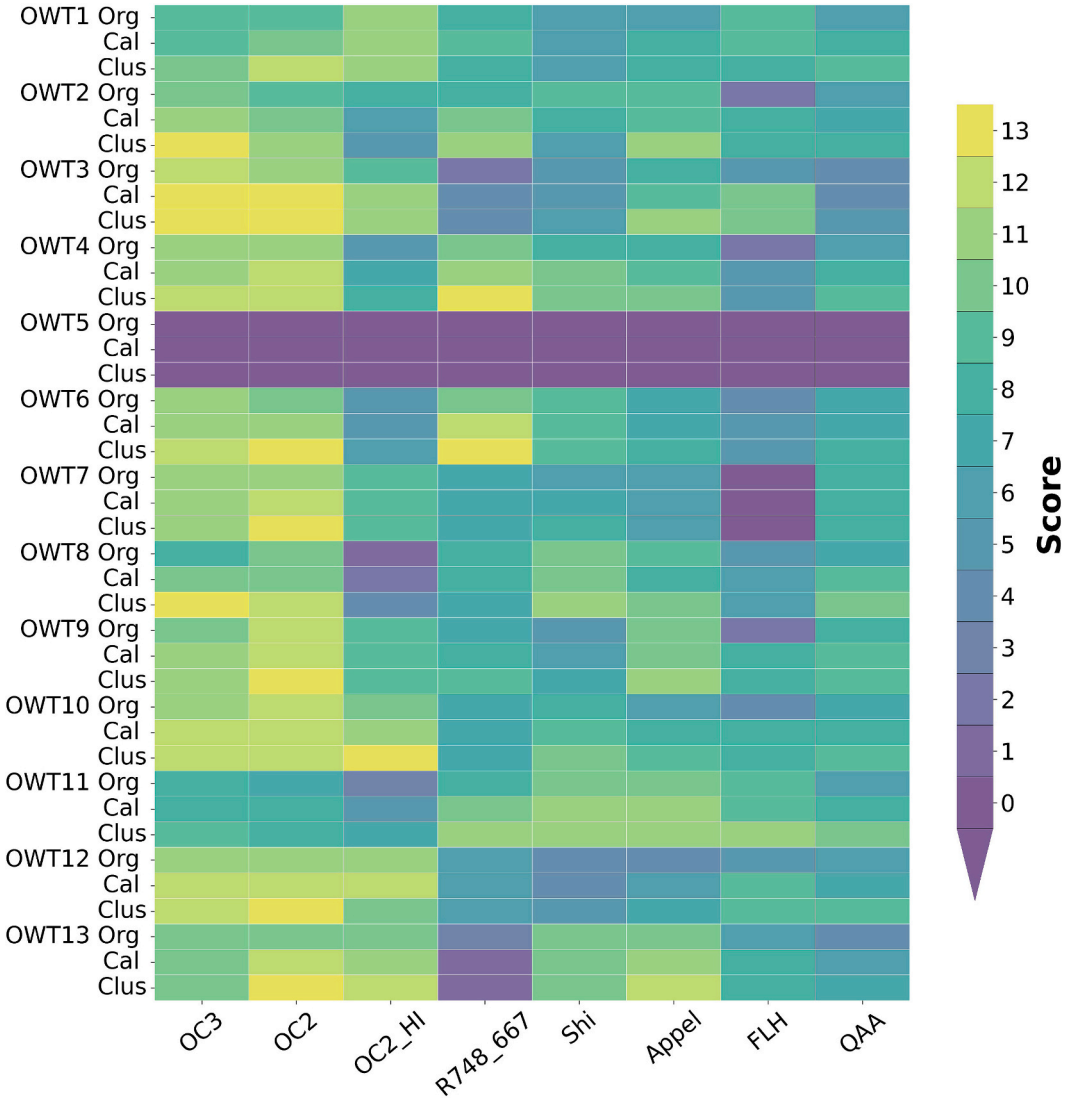

Fig. 7. OWT-specific performance of each evaluated chlorophyll-*a* algorithm.

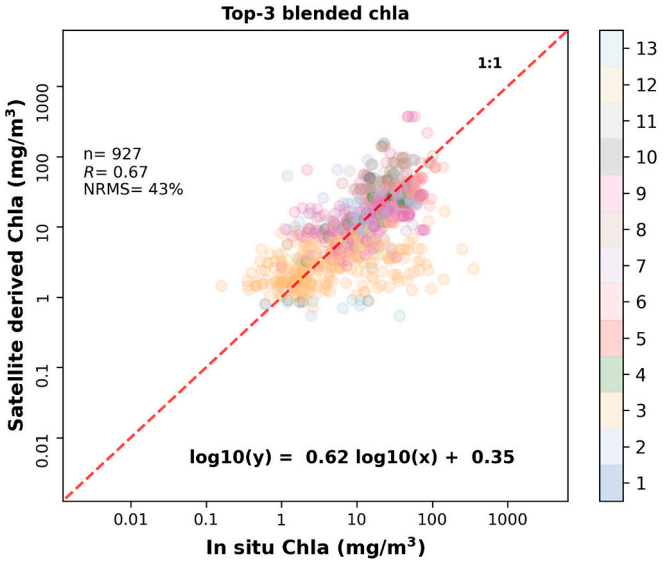

Fig. 8. Comparison between in situ and top-3 blended chlorophyll-*a* concentration for MODIS. Color coding refers to the most similar OWT.

MODIS and MERIS/OLCI.

3.5.2. *Example applications*

3.5.2.1. Time-series stability. To further illustrate the cross-sensor stability in time-series, the R_w(555) and Chl*a* products derived from all sensors over Lake Sevan, Chardarinskoye and the Razelm Lagoon are shown (Fig. 10 and Fig. 11). Chardarinskoye and Razelm Lagoon did not meet our subjective criteria for stability and were consequently not included among the 48 lakes selected for further analyses.

The time-series include 3-year overlapping periods between MODIS and MERIS, as well as MODIS and OLCI, respectively. The data represent the daily median observed values in these lakes as well as the 20th and 80th percentiles. The three lakes represent varying degrees of cross-sensor stability evaluated using correlation statistics. Lake Sevan showed acceptable inter-sensor stability, and it is clear from the time-series plots that MODIS R_w(555) captures the same seasonal patterns as observed with MERIS and OLCI, exhibiting strong correlation coefficients ($p < 0.001$, $R > 0.82$ and $T_{au} > 0.71$) between either MERIS or OLCI and MODIS (Fig. 10 a and a'). Similar patterns of variability and trends between the sensors are also seen for Chl*a* measurements (Fig. 11 a and a').

In Chardarinskoye moderate stability was observed across sensors.

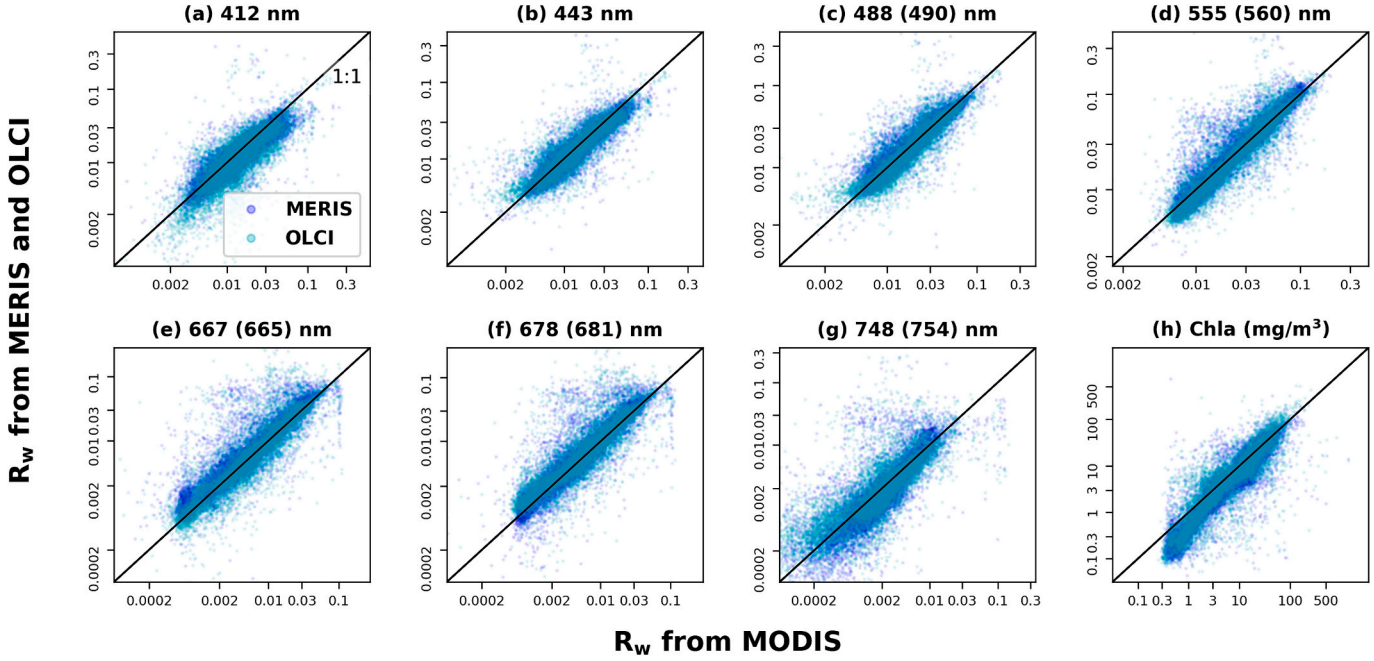

Fig. 9. Comparison of coincident observations between MODIS and MERIS or OLCI for (a-g) R_w wavebands and (h) chlorophyll-*a* concentration in 48 lakes for 3-year overlapping periods of 2009–2011 (MERIS) and 2017–2019 (OLCI), respectively. Only the R_w of the seven wavebands with <6 nm differences between MODIS and MERIS or OLCI are shown, with the MERIS or OLCI band indicated in parenthesis where it differs from the MODIS band.

Table 5
Descriptive statistics of satellite matchups between MERIS, OLCI, and MODIS in 48 lakes.

Sensors	MODIS vs MERIS (N = 11,571)					MODIS vs OLCI (N = 16,470)				
	R	Slope	RMSE	MAPE (%)	Bias	R	Slope	RMSE	MAPE (%)	Bias
412 nm	0.87	0.80	0.0097	20.2	−0.0024	0.80	0.87	0.0043	18.9	−0.0025
443 nm	0.89	0.86	0.0103	15.7	−0.0013	0.89	0.83	0.0027	11.6	−0.0010
488 (490) nm	0.91	0.89	0.0113	13.5	0.0009	0.90	0.93	0.0027	8.7	−0.0002
555 (560) nm	0.92	0.98	0.0119	13.2	0.0019	0.92	1.0	0.0040	9.3	0.0009
667 (665) nm	0.89	0.89	0.0133	44.1	0.0026	0.89	0.94	0.0043	29.4	0.0016
678 (681) nm	0.89	0.91	0.0131	39.7	0.0021	0.88	0.89	0.0044	32.3	0.0019
748 (754) nm	0.80	0.88	0.0077	52.0	0.0002	0.78	0.73	0.0027	40.8	0.0001
Chl*a*	0.80	0.86	7.1005	31.4	−2.201	0.87	1.00	9.3797	24.4	−0.7798
Average	0.87	0.90	/	28.7	/	0.87	0.90	/	21.9	/

Table 6
Comparative correlation statistics of MERIS, OLCI, and MODIS satellite matchups across 13 OWTs in all studied lakes for R_w555(560).

Sensors	MODIS vs MERIS (N = 66,282)							MODIS vs OLCI (N = 122,336)						
OWT	N (%)	N_return (%)	*R*	Slope	RMSE	MAPE (%)	Bias	N (%)	N_return (%)	R	Slope	RMSE	MAPE (%)	Bias
1	0.5	57.2	0.44	0.40	0.0146	21.38	−0.0053	1.4	58.7	0.45	0.41	0.0180	26.51	−0.0076
2	14.2	63.5	0.79	0.80	0.0192	8.12	0.0046	13.5	61.8	0.79	0.93	0.0219	9.45	0.0043
3	32.3	68.6	0.71	0.78	0.0187	9.69	0.0028	31.0	66.9	0.77	0.90	0.0158	9.47	−0.0010
4	7.7	58.8	0.76	0.76	0.0256	10.03	0.0058	7.9	59.1	0.80	0.89	0.0242	10.35	0.0069
5	0.9	44.7	0.40	0.50	0.2155	42.29	0.1429	2.5	46.0	0.36	0.40	0.1749	37.88	0.1047
6	3.0	61.4	0.76	0.74	0.0165	7.18	0.0046	1.9	56.3	0.77	0.74	0.0166	7.21	0.0013
7	0.2	52.3	0.36	0.40	0.0550	23.44	0.0090	0.1	48.9	0.52	0.50	0.0224	14.18	−0.0001
8	1.1	55.5	0.51	0.42	0.0347	13.89	0.0068	0.7	51.9	0.68	0.57	0.0194	10.01	−0.0017
9	17.6	64.3	0.78	0.84	0.0207	8.59	0.0037	18.1	62.4	0.77	0.92	0.0186	9.28	0.0008
10	2.3	52.0	0.48	0.40	0.0363	20.39	−0.0001	6.1	50.0	0.49	0.32	0.0308	20.43	0.0038
11	6.9	55.2	0.68	0.67	0.0267	12.33	0.0033	6.0	53.1	0.75	0.74	0.0259	11.80	0.0049
12	0.5	62.2	0.54	0.65	0.0687	18.35	0.0096	1.4	63.4	0.65	0.74	0.0412	17.87	−0.0020
13	12.9	62.9	0.36	0.45	0.0256	15.91	0.0065	9.4	63.0	0.57	0.63	0.0216	12.10	−0.0013

MODIS R_w(555) successfully captured the same seasonal patterns observed with MERIS and OLCI, with moderate R values of ~0.60, and T_{au} value of ~0.5 found with MERIS and OLCI (Fig. 10 b and b'). MODIS-derived Chl*a* data also demonstrated broadly similar seasonal trends to those observed with MERIS and OLCI, despite larger discrepancies on specific dates (Fig. 11 b and b'). In contrast, Razelm Lagoon exhibited poor stability between sensors in both R_w(555) and Chl*a* products, with weak correlations ($p < 0.001$, $R < 0.25$ and $T_{au} < 0.1$).

3.5.2.2. Spatial stability. Overlapping scenes of MODIS with MERIS or

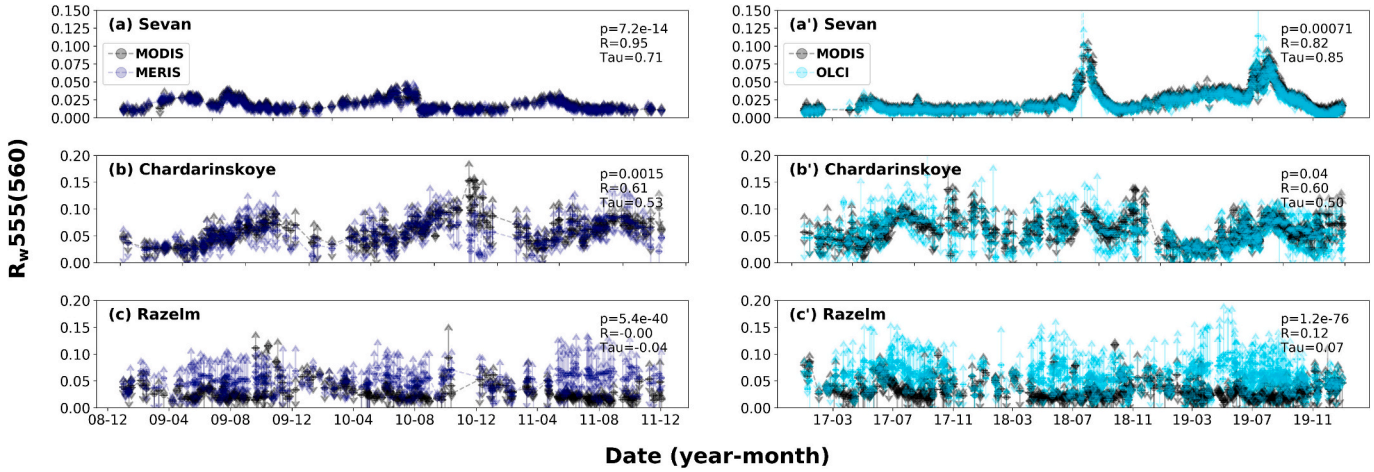

Fig. 10. Comparative analysis of inter-sensor stability for R_w555(560): (a-c) MERIS *vs.* MODIS (2009–2011) and (a'-c') OLCI *vs.* MODIS (2017–2019) in Lake Sevan, Chardarinskoye, and Razelm Lagoon.

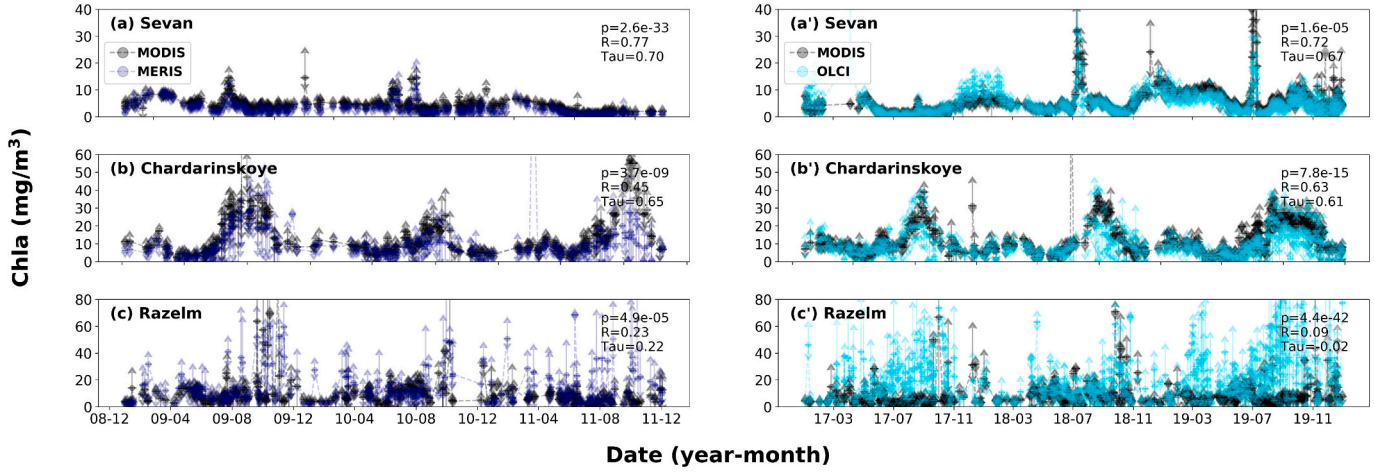

Fig. 11. Comparative analysis of inter-sensor stability for chlorophyll-*a* concentration: (a-c) MERIS *vs.* MODIS (2009–2011) and (a'-c') OLCI *vs.* MODIS (2017–2019) in Lake Sevan, Chardarinskoye, and Razelm Lagoon.

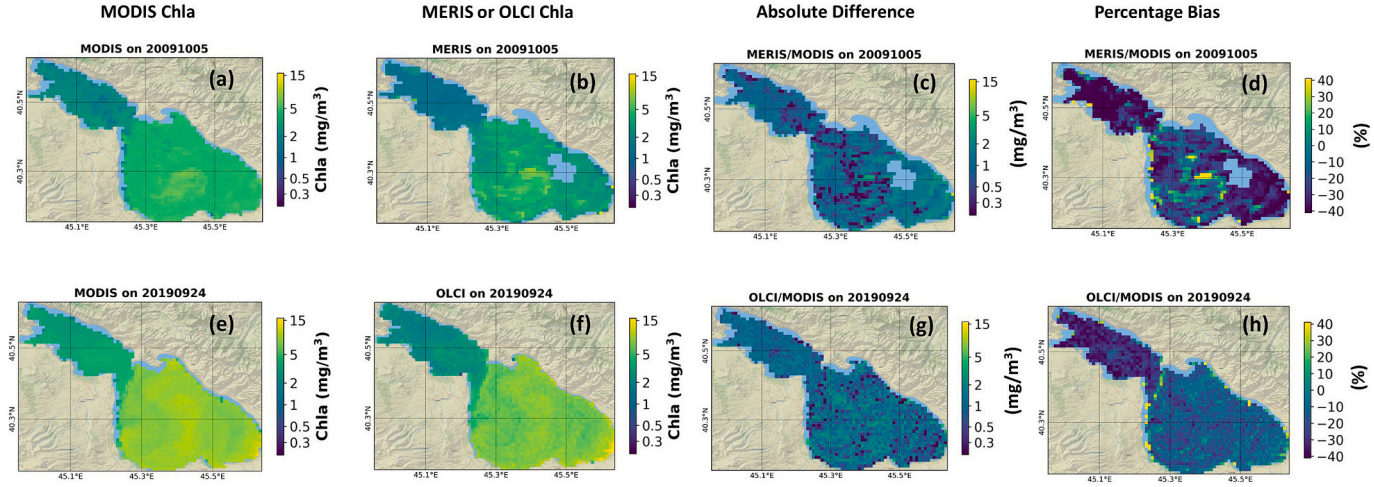

Fig. 12. Inter-sensor comparison of chlorophyll-*a* maps in Lake Sevan. The Absolute Difference and Percentage Bias maps are shown comparing either MERIS or OLCI to MODIS.

OLCI under clear sky were selected to evaluate stability in spatial patterns of Chl*a* in lake Sevan on dates of 5th Oct 2009 and 24th Sep 2019, respectively. MODIS-derived Chl*a* showed similar spatial patterns as observed with MERIS and OLCI, with lower Chl*a* observed in the northwest part of the lake and higher Chl*a* retrievals in the southeast (Fig. 12). The lake average value of Absolute Difference (AD) and Percentage Bias (PB) for MERIS vs MODIS were − 0.9 and − 24.9%, compared to −0.9 and − 16.7% for OLCI vs MODIS. Negative PB was found in the regions with low Chl*a* concentrations (<2 mg/m^3), which indicates a protentional overestimation of MODIS compared to MERIS and OLCI in low Chl*a* ranges (Fig. 12).

3.5.2.3. Lake regime shifts in a changing climate. As a demonstration of the gap-free long-term satellite observation, Fig. 13 shows the inter-annual trend of LWL, LWST, and Chl*a* in lake Sevan, after removing the seasonal component from the time-series satellite observations. In lake Sevan, measures were taken by the local government since 2002 to increase the LWL in order to restore the natural regime of the lake water (Hovsepyan et al., 2019), which is captured by the LWL retrievals provided in the lakes_cci dataset (Fig. 13a). With the increase of the LWL, the tendency of a decrease in Chl*a* was registered and maintained at a low value from 2010 to 2016 (Fig. 13a and c). While in recent years, the Chl*a* trend has been gradually increasing and maintained at a high-level from 2017 to 2020. A reported massive blooming event that occurred in 2018 (Gevorgyan et al., 2020) was also confirmed by our Chl*a* product, which could be related to the sudden increase in water temperature in 2018 (Fig. 13 a and c).

4. Discussion

Reliable, continuous, and long-term satellite observation records complement the management of lakes and are essential to identify and address the challenges of mitigating and adapting to climate change acting on water bodies and their catchments. Multi-decadal observation of optical proxies for lake biogeochemistry has been hampered by a crucial observation gap between the MERIS and OLCI satellite sensors. These sensors have otherwise prompted considerable advances towards fulfilling the Lakes Essential Climate Variable, particularly by complementing the waveband set of previous generations of sensors in the near-infrared and by providing a nominal pixel resolution of 300 m to further the study of medium-sized lakes. As a result of the observation gap, studies of inland optical water quality have predominantly focused on the period of either MERIS or OLCI observations (Kauer et al., 2015; Liu et al., 2019; Qian et al., 2022). The present work provides the first indirect evaluation of MERIS and OLCI long-term stability using the overlapping temporal coverage by MODIS-Aqua.

As one of the most limiting factors for accurate retrieval of water-leaving reflectance from satellite remote sensing data, atmospheric correction over inland waters is often found unreliable compared to ocean color remote sensing, due to the optical complexity and variability of water constituents even under optimal observing conditions (cloud-free, thin aerosols, negligible sun glint) (Moses et al., 2009; Warren et al., 2019). For the two AC algorithms considered in this study, we find that atmospherically corrected R_w was systematically lower than in situ observations (Fig. 4), which is consistent with results reported in other studies (Jiang et al., 2020; Soppa et al., 2021). This behavior is not unique to the correction of MODIS-Aqua imagery, and inter-sensor comparison results of water-leaving radiance reflectance suggest that similar agreement is found between MODIS-Aqua and MERIS in the period up until 2012, and between MODIS-Aqua and OLCI A/B for the period starting from 2016. These findings, while acknowledging the presence of observation uncertainties, suggest a possible continuity between the MERIS and OLCI sensor products when integrated with MODIS-Aqua, and potentially to include legacy sensors such as SeaWIFS to further extend the observation time series.

A major factor in determining the most suitable satellite data processing chain is the degree to which observations of sufficient quality are preserved whilst masking out observations of poor quality. POLYMER

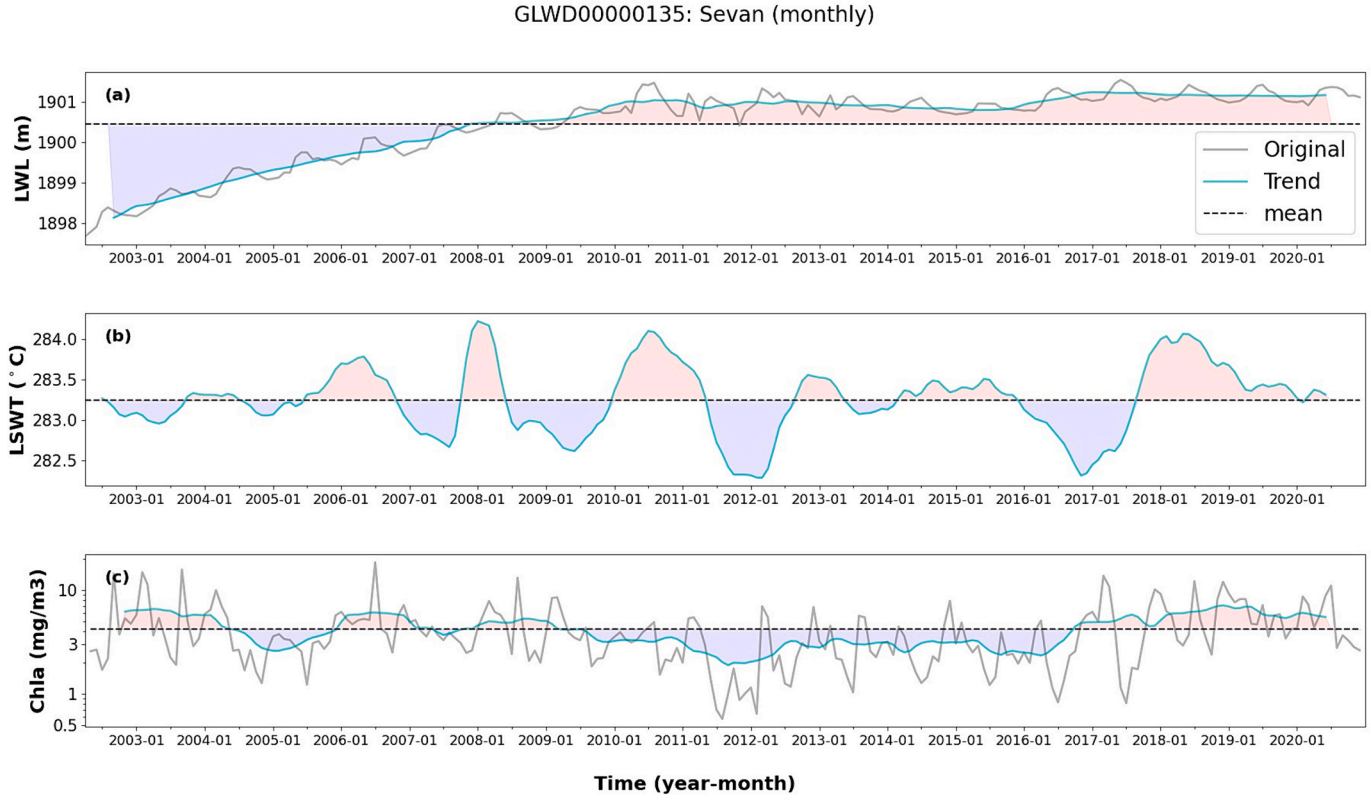

Fig. 13. De-seasonalized trend of (a) Lake Water Level, (b) Lake Surface Water Temperature, and (c) chlorophyll-*a* concentration in lake Sevan from 2002 to 2020.

yields are almost two-fold the number of valid pixels compared to L2gen whilst providing similar performance. Similar findings are reported in a comparison of POLYMER and the NASA standard atmospheric correction (NSAC) applied to MODIS measurements over North American waters (Zhang et al., 2018), where POLYMER retrieved 2–3 fold more valid observations than NSAC. This property of POLYMER is also reported for other sensors such as OLCI, when evaluated among five AC algorithms over French optically complex waters (Mograne et al., 2019). The availability of valid ocean observations from MODIS (e.g., R_w and Chl*a*) can be as low as ~5% (Feng and Hu, 2015), suggesting approximately 1 valid pixel from every 20 days over the same location, given the daily revisit frequency of MODIS-Aqua. For inland waters, this value should be adjusted downward due to the complexity of variable aerosol and water properties. POLYMER works relatively effectively in the presence of thin clouds and sun glint, increasing the valid coverage of satellite measurements in challenging conditions, making it a good choice to observe the dynamic nature of inland waters due to precipitation events, river dynamics, wind-driven resuspension, and anthropogenic pollution.

The 48 lakes presently encompassed in the Lakes_cci have yielded a reasonable degree of stability between MERIS, OLCI and MODIS, thereby providing a level of confidence to achieve longer time series by combining observations from these sensors (Fig. 9 and Table 5), especially considering blue and green bands from 443 to 555 nm. Generally better agreement between MODIS and OLCI was found for R_w between blue and green bands (from 443 to 555 nm) than between MODIS and MERIS (Table 5). A study on inter-calibration of the cyanobacteria index (CI) from MERIS, MODIS, and OLCI in the Laurentian Great lakes also showed slightly better agreement between OLCI and MODIS-derived CI than that between MERIS and MODIS (Wynne et al., 2021).

Nevertheless, the dynamic range of the MODIS instrument aboard the Terra and Aqua satellites is limited at both ends of the dynamic scale due to quantization noise at the low end and limited amplifier capacity at the high end. Specific detectors in the MODIS instruments exhibit a tendency to reach saturation early due to the detector material properties: bands 15 (748 nm), 17 (905 nm), and 19 (940 nm) can experience pre-saturation at approximately 92%, 81%, and 90% of the dynamic range (Madhavan et al., 2012). Evidence of saturation in the wider green to near -infrared wavelength region has also been shown over highly turbid waters (Li et al., 2017; Madhavan et al., 2012). In our study, the N_return of MODIS observations was above 55% for the majority of OWTs when compared to MERIS and OLCI data (Table 6). The generally lower pixel returned by MODIS is likely due to its coarser spatial resolution (1 km) compared to the finer 300 m resolution provided by MERIS and OLCI. Notably, OWTs 5 (characterized by high sediment content), 7 (high Chl*a* and phycocyanin concentration) and 10 (rich in CDOM) exhibited slightly lower N_return, ranging from 44.7% to 52.3%, when compared to other OWTs. This reduced rate of N_return for these OWTs could be associated with MODIS band saturation issues specific to these water types, which suggests a need for further detailed investigation to draw definitive conclusions.

Among the example lakes shown in our study, the observed poor stability in Razelm Lagoon (Fig. 11) may be attributed to its shallow depth (1.9 m) and generally turbid conditions, which arise from sediment resuspension and algae blooms (Godeanu and Galatchi, 2007; Navodaru et al., 2002). Razelm Lagoon has an average Chl*a* concentration of 208.2 mg/m^3 (ranging from 3.5 to 1046 mg/m^3) and an average water transparency of 0.26 m (ranging from 0.19 to 0.42 m), based on monthly surveys conducted over 12 years from 1993 to 2005 (Godeanu and Galatchi, 2007). Consequently, MODIS bands tend to saturate in this lake, resulting in fewer valid pixels and a resulting bias towards occurrences of lower values in time series for both R_w and Chl*a*, compared to MERIS and OLCI.

The saturation of several MODIS wavebands in highly turbid waters presents a specific challenge to present consistent long-term time-series without significant bias to more favourable conditions. Research suggests that the 'land' bands on MODIS are less affected by saturation in these conditions, and could be used as alternatives for Chl*a* estimates in areas with extreme turbidity and high biomass (Li et al., 2019; Qi et al., 2014). Despite the potential of land bands for Chl*a* estimation in turbid waters, their broader spectral resolution and lower sensitivity pose significant challenges for globally applicable algorithm development. Recent studies have nevertheless indicated potential for MODIS land bands to assess water clarity and extinction coefficients across a wider range of water bodies, while quantifying Chl*a* in estuarine and inland waters using MODIS land bands remains challenging (Cao et al., 2022).

Relatively consistent R_w observations between MERIS, OLCI, and MODIS-Aqua across their shared bandset do not imply that Chl*a* concentration estimates will be of similar quality, because MERIS and OLCI benefit from additional wavebands which can be exploited in Chl*a* retrieval. Moreover, additional bands corresponding to atmospheric features are expected to improve atmospheric correction of visible and near-infrared signals. Some of the most successful and widely applicable Chl*a* algorithms for MERIS make use of near-infrared bands (Neil et al., 2019). Other algorithm candidates such as the OCX family of algorithms operate on the blue and green wavebands, and are considered most appropriate for relatively clear (oligotrophic and mesotrophic) water types.

Interestingly, the OCX algorithms showed generally better performance than the other evaluated algorithms for most of the OWTs in this study (Fig. 4 and Fig. 5). The R748/667 algorithm showed superior performance for the three OWTs (4, 6 and 11) with the highest Chl*a* concentrations, which is conform expectations (Fig. 3 and Table 4). The relative performance of the OCX algorithm contrasts the common finding that algorithms using Red/NIR wavebands tend to perform better across a wide range of optically complex inland waters, and may be related to superior retrieval of the near-infrared R_w signal from MERIS and OLCI, compared to MODIS, after atmospheric correction. Another possible reason for the lesser performance of algorithms employing Red/NIR bands could be tied to the fact that MODIS Red/NIR bands (e.g., 667, 678, and 748 nm) are more intend to encounter band saturation issues, particularly in extremely turbid waters including dense algal blooms. This, in turn, impedes the successful application of algorithms utilizing these bands (e.g., algorithms R748/667, FLH). Classic atmospheric correction methods often fail in turbid waters since the backscattering in the NIR overcomes the high light absorption efficiency by water molecules, invalidating the black-pixel assumption in the NIR (Shi and Wang, 2007). Despite the successful application of the MODIS SWIR atmospheric correction method for some turbid waters (Ibrahim et al., 2019; Shi and Wang, 2007; Wang et al., 2009), this approach no longer holds for extremely turbid waters (Shi and Wang, 2007; Wang et al., 2019). Given that MODIS sensors are primarily designed for the observation of oceanic waters, and the lack of MODIS wavebands in the NIR/SWIR compared to MERIS and OLCI, it is reasonable to observe a lack of adequate accuracy for Chl*a* algorithms using red or NIR wavebands, which are also widely used in the retrieval of TSM. This observation was further corroborated by some additional unsuccessful attempts conducted on TSM retrieval (Simis et al., 2022), which confirmed the aforementioned limitation of MODIS in this regard.

Other studies have shown that OCX algorithms are likely to give erroneous estimates in extremely turbid waters by an overestimation in Chl*a* concentrations, or an underestimation of Chl*a* in hyper-eutrophic waters (Camiolo et al., 2016; Tilstone et al., 2017). The tuning process actively reduced the underestimation in the high Chl*a* section by improving the linear-regression slope for OC3 (from 0.5 to 0.6) and OC2 (from 0.52 to 0.6) (Fig. 5). Our study has confirmed the finding of other studies that find that MODIS could provide a consistent measurement of algal bloom products with that of MERIS and OLCI (Wynne et al., 2021; Zeng and Binding, 2021).

In our study, we discovered that MODIS can be used for gap-filling in climate studies across certain lakes, although it does not present a universal solution for all lakes. The primary limitation of MODIS is the size

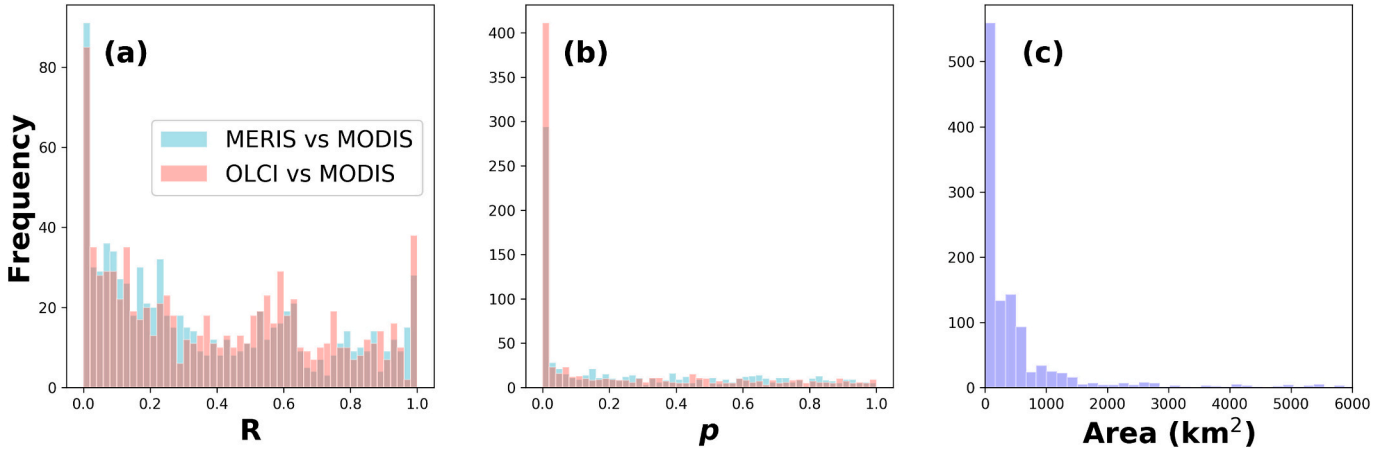

Fig. 14. Histograms illustrating comparative analysis: (a) determination coefficients and (b) *p*-values for satellite-derived chlorophyll-*a* concentrations among MERIS, OLCI, and MODIS across evaluated lakes, and (c) distribution of lake areas.

of the lakes for which it achieves consistent results. A significant portion of the lakes examined in our study—603 out of a total of 1167—are <200 km^2 in size (Fig. 14c), which complicates the achievement of consistent observations between MERIS/OLCI and MODIS due to the discrepancy in spatial resolutions between these sensors. This challenge is further exacerbated in cases where lakes exhibit irregular shapes, presenting additional obstacles for MODIS satellite observation, which has a spatial resolution of 1 km for ocean color bands. By broadening the selection criterion to $R > 0.4$ across the three sensors, the number of lakes passing the stability check increases to approximately 80 (Fig. 14).

Climate change significantly impacts on inland water ecosystems, but it will be difficult to distinguish climate-induced and natural variability among other pressures without substantially longer data records than have been available to date. In the application example presented here, the responses of Chl*a* to physical changes (in LWL and LSWT) in Lake Sevan confirm the effectiveness of the gap-filled time-series satellite data (Fig. 13). It is worth noting that both LWL and LSWT products are freely accessible in the same format as the LWLR data from the Lakes_cci project (https://climate.esa.int/en/projects/lakes/data/). Therefore, similar analyses can be carried out in lakes where MODIS Chl*a* products are available to study the long-term variation of Chl*a*, and investigate how it responds to variations in lake hydrologic and climatic conditions.

MODIS, with its long operational period, offers a unique opportunity to bridge the temporal gap between the MERIS and OLCI missions, ensuring data continuity for long-term environmental monitoring. Despite spectral and spatial resolution differences among the three sensors, their overlapping bands can be harmonized for consistent datasets in relatively large lakes. However, challenges arise due to algorithm variations, waveband discrepancies, and differing spatial resolutions. In our study, substantial efforts were directed towards identifying a well-performing atmospheric correction algorithm, calibrating Chl*a* algorithms within an OWT-based framework, and identifying lakes that could yield acceptably consistent data across the three sensors. Looking ahead, to effectively amalgamate data from MERIS, MODIS, and OLCI, and to extend this work to encompass more lakes, rigorous inter-calibration, algorithm harmonization, and validation utilizing in-situ measurements are indispensable. Furthermore, due to the large uncertainty associated with atmospheric correction, analysis and potential reduction of the correction error should include analysis of atmospheric composition as far as this is possible through observation and simulation studies, to arrive at a full propagation of uncertainties instead of strict masking of suspect observations.

5. Conclusions

In this study, MODIS Chl*a* algorithms were individually tuned against in situ observations, grouped by their similarity to an established set of optical water types. The calibration of algorithms within the scope of individual optical water types is considered particularly beneficial when the satellite sensor is not optimally equipped to address the compound challenges of atmospheric correction over optically complex water in the vicinity of land. Although systemic underestimation of MODIS R_w was observed for both AC algorithms, the re-calibrated Chl*a* algorithms can cancel out some of the R_w bias, particularly when algorithms determine the Chl*a* from band ratios. Following the process of calibration per optical water type, the agreement between MODIS and OLCI derived Chl*a* was slightly better than between MODIS and MERIS, indicating that a further refinement of algorithms, and ultimately inter-sensor bias correction might prove useful to obtain seamless gap-filled time-series. This continued fine-tuning is facilitated by continued efforts to uncover and share in situ radiometric and biogeochemical observation data, serving to determine the product uncertainties associated with estimates derived from the individual sensors.

CRediT authorship contribution statement

Xiaohan Liu: Writing – original draft, Visualization, Formal analysis, Conceptualization. **Mark Warren:** Writing – review & editing, Data curation. **Nick Selmes:** Writing – review & editing, Data curation. **Stefan G.H. Simis:** Writing – review & editing, Funding acquisition, Conceptualization.

Declaration of competing interest

The authors declare that they have no known competing financial interests or personal relationships that could have appeared to influence the work reported in this paper.

Data availability

In situ data used were requested through the LIMNADES database, curated by the University of Stirling. Satelite products produced for this study are available through the Lakes_cci project.

Acknowledgments

All in situ datasets for this research are sourced from the in situ bio-optical data repository LIMNADES (Lake Bio-optical Measurements and Matchup Data for Remote Sensing: https://limnades.stir.ac.uk)

maintained by the University of Stirling. The Chl*a* product for global lakes based on the methodology proposed in this study are available from the ESA Lakes Climate Change Initiative (Lakes_cci): Lake products, Version 2.0.2 (https://climate.esa.int/en/projects/lakes/data/). The authors acknowledge funding from the ESA Lakes Climate Change Initiative project. We also thank all organizations and individuals who made in situ data available through LIMNADES under the GloboLakes project and separate agreements: Agri-food and Biosciences Institute in Northern Ireland; General Directorate of Water Management (OVF, Hungary); Central Transdanubian Inspectorate for Environmental and Natural Protection (Közép-dunántúli Környezetvédelmi és Természetvédelmi Felügyelőség); Balaton Limnological Institute; Finnish Environment Institute; Mariano Bresciani and Claudia Giardino (Institute for Electromagnetic Sensing of the Environment, CNR-IREA, Milano, Italy); Anatoly A. Gitelson (Department of Civil and Environmental Engineering, Israel Institute of Technology, Technion City, Haifa, Israel); Tiit Kutser (Estonian Marine Institute, University of Tartu, Tallinn, Estonia); Bunkei Matsushita (Faculty of Life and Environmental Sciences, University of Tsukuba, Ibaraki, Japan); Mark W. Matthews (CyanoLakes (Pty) Ltd., Cape Town, South Africa).

Appendix A. Appendix

(a) OC2 algorithm.

The OC2 algorithm relies on a ratio of blue (488) and green (547) wavebands. The algorithm is formulated as:

$$Chla = 10^{\left(p_0+\sum_{i=1}^{4} p_i\left(log_{10}\left(\frac{R_w(488)}{R_w(547)}\right)\right)^i\right)} \tag{A1}$$

where p_0 to p_5 are tuned constants. The OC2 algorithm is assigned to OWTs 1, 5, 7, 9, 12, and 13, and the calibrated coefficients are shown in Table A1.

(b) OC3 algorithm.

The OC2 algorithm relies on a maximum ratio of blue (443, 488) to green (547) wavebands. The algorithm is formulated as:

$$Chla = 10^{\left(p_0+\sum_{i=1}^{4} p_i(X)^i\right)} \tag{A2}$$

$$X = log10((R_w(443) > R_w(488))/R_w(547)) \tag{A3}$$

where p_0 to p_5 are tuned constants. The OC2 algorithm is assigned to OWTs 2, 3, and 8, the calibrated coefficients are shown in Table A1.

(c) R748_667 algorithm.

The Dall'Olmo et al. (2005) algorithm is an empirically tuned ratio of bands 748 and 667 nm:

$$Chla = 10^{p_0+p_1\times log_{10}(ratio)} + p_2 \tag{A4}$$

Where p_0 to p_3 are tuning coefficients empirically calibrated against LIMNADES. The R748_667 algorithm is assigned to OWTs 4, 6 and 11, the calibrated coefficients are shown in Table A1.

(d) OC2_HI algorithm.

The OC2_HI algorithm relies on a ratio of blue (469) and green (555) wavebands. The algorithm is formulated as:

$$Chla = 10^{\left(p_0+\sum_{i=1}^{4} p_i\left(log_{10}\left(\frac{R_w(469)}{R_w(555)}\right)\right)^i\right)} \tag{A5}$$

where p_0 to p_5 are tuned constants. The OC2_HI algorithm is assigned to OWTs 10, the calibrated coefficients are shown in Table A1.

Table A1
Per-OWT tuned parameters for each assigned Chl*a* algorithms.

Algorithm	Assigned OWT	p_0	p_1	p_2	p_3	p_4
OC2	1	0.2750	−2.7227	1.5467	−3.1056	0.5945
OC2	5	0.2875	−2.8465	1.6170	−3.2468	0.6216
OC2	7	0.2750	−2.7227	1.5467	−3.1056	0.5946
OC2	9	0.2875	−2.7419	1.3401	−2.5856	0.5996
OC2	12	0.2750	−2.7227	1.5467	−3.0026	0.4918
OC2	13	0.2731	−2.7227	1.5467	−2.7567	0.4865
OC3	2	0.2252	−3.2904	1.5478	0.0018	−1.4736
OC3	3	0.1939	−3.0978	1.8570	0.0012	−1.2255
OC3	8	0.2901	−3.2908	2.1620	0.0012	−0.9824
R748_667	4	2.0075	1.6560	−2.0352	\	\
R748_667	6	1.9995	1.5870	−2.9537	\	\

(*continued on next page*)

Table A1 (*continued*)

Algorithm	Assigned OWT	p_0	p_1	p_2	p_3	p_4
R748_667	11	2.1495	1.5194	−6.4474	\	\
OC2_HI	10	0.1171	−1.9706	1.1662	−0.9983	−0.6458

References

Adrian, R., O'Reilly, C.M., Zagarese, H., Baines, S.B., Hessen, D.O., Keller, W., Livingstone, D.M., Sommaruga, R., Straile, D., Van Donk, E., 2009. Lakes as sentinels of climate change. Limnol. Oceanogr. 54, 2283–2297.

Attila, J., Kauppila, P., Kallio, K.Y., Alasalmi, H., Keto, V., Bruun, E., Koponen, S., 2018. Applicability of earth observation chlorophyll-a data in assessment of water status via MERIS—with implications for the use of OLCI sensors. Remote Sens. Environ. 212, 273–287.

Bailey, S.W., Franz, B.A., Werdell, P.J., 2010. Estimation of near-infrared water-leaving reflectance for satellite ocean color data processing. Opt. Express 18, 7521–7527.

Bhagowati, B., Ahamad, K.U., 2019. A review on lake eutrophication dynamics and recent developments in lake modeling. Ecohydrol. Hydrobiol. 19, 155–166.

Camiolo, M.D., Cozzolino, E., Simionato, C.G., Hozbor, M.C., Lasta, C.Á., 2016. Evaluating the performance of the OC5 algorithm of IFREMER for the highly turbid waters of Río de la Plata. Braz. J. Oceanogr. 64, 19–28.

Cao, Z., Shen, M., Kutser, T., Liu, M., Qi, T., Ma, J., Ma, R., Duan, H., 2022. What water color parameters could be mapped using MODIS land reflectance products: a global evaluation over coastal and inland waters. Earth Sci. Rev. 104154.

Carlson, R.E., Simpson, J., 1996. A coordinator's guide to volunteer lake monitoring methods, p. 305.

Dall'Olmo, G., Gitelson, A.A., Rundquist, D.C., Leavitt, B., Barrow, T., Holz, J.C., 2005. Assessing the potential of SeaWiFS and MODIS for estimating chlorophyll concentration in turbid productive waters using red and near-infrared bands. Remote Sens. Environ. 96, 176–187.

Donlon, C., Berruti, B., Buongiorno, A., Ferreira, M.-H., Féménias, P., Frerick, J., Goryl, P., Klein, U., Laur, H., Mavrocordatos, C., 2012. The global monitoring for environment and security (GMES) sentinel-3 mission. Remote Sens. Environ. 120, 37–57.

El-Alem, A., Chokmani, K., Laurion, I., El-Adlouni, S.E., 2012. Comparative analysis of four models to estimate schlorophyll-a concentration in case-2 waters using MODerate resolution imaging spectroradiometer (MODIS) imagery. Remote Sens. 4, 2373–2400.

Feng, L., Hu, C., 2015. Comparison of valid ocean observations between MODIS Terra and Aqua over the global oceans. IEEE Trans. Geosci. Remote Sens. 54, 1575–1585.

Gevorgyan, G., Rinke, K., Schultze, M., Mamyan, A., Kuzmin, A., Belykh, O., Sorokovikova, E., Hayrapetyan, A., Hovsepyan, A., Khachikyan, T., 2020. First report about toxic cyanobacterial bloom occurrence in Lake Sevan, Armenia. Int. Rev. Hydrobiol. 105, 131–142.

Gitelson, A., 1992. The peak near 700 nm on radiance spectra of algae and water: relationships of its magnitude and position with chlorophyll concentration. Int. J. Remote Sens. 13, 3367–3373.

Gitelson, A.A., Schalles, J.F., Hladik, C.M., 2007. Remote chlorophyll-a retrieval in turbid, productive estuaries: Chesapeake Bay case study. Remote Sens. Environ. 109, 464–472.

Gitelson, A.A., Dall'Olmo, G., Moses, W., Rundquist, D.C., Barrow, T., Fisher, T.R., Gurlin, D., Holz, J., 2008. A simple semi-analytical model for remote estimation of chlorophyll-a in turbid waters: validation. Remote Sens. Environ. 112, 3582–3593.

Godeanu, S., Galatchi, L., 2007. The determination of the degree of eutrophication of the lakes on the Romanian seaside of the Black Sea. In: Annales de Limnologie-International Journal of Limnology. EDP Sciences, pp. 245–251.

Gurlin, D., Gitelson, A.A., Moses, W.J., 2011. Remote estimation of chl-a concentration in turbid productive waters—return to a simple two-band NIR-red model? Remote Sens. Environ. 115, 3479–3490.

Ha, N.T.T., Koike, K., Nhuan, M.T., 2013. Improved accuracy of chlorophyll-a concentration estimates from MODIS imagery using a two-band ratio algorithm and geostatistics: as applied to the monitoring of eutrophication processes over Tien Yen Bay (Northern Vietnam). Remote Sens. 6, 421–442.

Hovsepyan, A., Mamyan, A., Khachikyan, T., Tikhonova, I., Belykh, O., Gevorgyan, G., 2019. Monitoring of phytoplankton status in Lake Sevan (Armenia) in 2018. Proc. YSU: Chem. Biol. Sci. 53, 206–211.

Ibrahim, A., Franz, B.A., Ahmad, Z., Bailey, S.W., 2019. Multiband atmospheric correction algorithm for ocean color retrievals. Front. Earth Sci. 7, 116.

Jiang, L., Guo, X., Wang, L., Sathyendranath, S., Evers-King, H., Chen, Y., Li, B., 2020. Validation of MODIS Ocean-colour products in the coastal waters of the Yellow Sea and East China Sea. Acta Oceanol. Sin. 39, 91–101.

Kasprzak, P., Padisák, J., Koschel, R., Krienitz, L., Gervais, F., 2008. Chlorophyll a concentration across a trophic gradient of lakes: an estimator of phytoplankton biomass? Limnologica 38, 327–338.

Kauer, T., Kutser, T., Arst, H., Danckaert, T., Nõges, T., 2015. Modelling primary production in shallow well mixed lakes based on MERIS satellite data. Remote Sens. Environ. 163, 253–261.

Kirk, J.T.O., 2011. Light and Photosynthesis in Aquatic Ecosystems, 3nd ed. Cambridge University Press, New York.

Kratzer, S., Brockmann, C., Moore, G., 2008. Using MERIS full resolution data to monitor coastal waters—a case study from Himmerfjärden, a fjord-like bay in the northwestern Baltic Sea. Remote Sens. Environ. 112, 2284–2300.

Kruse, F.A., Lefkoff, A., Boardman, J., Heidebrecht, K., Shapiro, A., Barloon, P., Goetz, A., 1993. The spectral image processing system (SIPS)—interactive visualization and analysis of imaging spectrometer data. Remote Sens. Environ. 44, 145–163.

Letelier, R.M., Abbott, M.R., 1996. An analysis of chlorophyll fluorescence algorithms for the moderate resolution imaging spectrometer (MODIS). Remote Sens. Environ. 58, 215–223.

Li, J., Hu, C., Shen, Q., Barnes, B.B., Murch, B., Feng, L., Zhang, M., Zhang, B., 2017. Recovering low quality MODIS-Terra data over highly turbid waters through noise reduction and regional vicarious calibration adjustment: a case study in Taihu Lake. Remote Sens. Environ. 197, 72–84.

Li, J., Gao, M., Feng, L., Zhao, H., Shen, Q., Zhang, F., Wang, S., Zhang, B., 2019. Estimation of chlorophyll-a concentrations in a highly turbid eutrophic lake using a classification-based MODIS land-band algorithm. IEEE J. Sel. Top. Appl. Earth Obs. Remote Sens. 12, 3769–3783.

Liu, X., Lee, Z., Zhang, Y., Lin, J., Shi, K., Zhou, Y., Qin, B., Sun, Z., 2019. Remote sensing of secchi depth in highly turbid lake waters and its application with MERIS data. Remote Sens. 11, 2226.

Liu, X., Steele, C., Simis, S., Warren, M., Tyler, A., Spyrakos, E., Selmes, N., Hunter, P., 2021. Retrieval of chlorophyll-a concentration and associated product uncertainty in optically diverse lakes and reservoirs. Remote Sens. Environ. 267, 112710.

Madhavan, S., Angal, A., Dodd, J., Sun, J., Xiong, X., 2012. Analog and digital saturation in the MODIS reflective solar bands. In: Earth Observing Systems XVII. SPIE, pp. 641–651.

Maritorena, S., Siegel, D.A., Peterson, A.R., 2002. Optimization of a semianalytical ocean color model for global-scale applications. Appl. Opt. 41, 2705–2714.

Meister, G., Franz, B.A., 2014. Corrections to the MODIS Aqua calibration derived from MODIS Aqua Ocean color products. IEEE Trans. Geosci. Remote Sens. 52, 6534–6541.

Miller, R.L., McKee, B.A., 2004. Using MODIS Terra 250 m imagery to map concentrations of total suspended matter in coastal waters. Remote Sens. Environ. 93, 259–266.

Mobley, C.D., Mobley, C.D., 1994. Light and Water: Radiative Transfer in Natural Waters. Academic press.

Mograne, M.A., Jamet, C., Loisel, H., Vantrepotte, V., Mériaux, X., Cauvin, A., 2019. Evaluation of five atmospheric correction algorithms over French optically-complex waters for the sentinel-3A OLCI Ocean color sensor. Remote Sens. 11, 668.

Moses, W.J., Gitelson, A.A., Berdnikov, S., Povazhnyy, V., 2009. Estimation of chlorophyll-a concentration in case II waters using MODIS and MERIS data—successes and challenges. Environ. Res. Lett. 4, 045005.

Navodaru, I., Buijse, A.D., Staras, M., 2002. Effects of hydrology and water quality on the fish communityin Danube delta lakes. Int. Rev. Hydrobiol. 87, 329–348.

Neil, C., Spyrakos, E., Hunter, P.D., Tyler, A.N., 2019. A global approach for chlorophyll-a retrieval across optically complex inland waters based on optical water types. Remote Sens. Environ. 229, 159–178.

Odermatt, D., Gitelson, A., Brando, V.E., Schaepman, M., 2012. Review of constituent retrieval in optically deep and complex waters from satellite imagery. Remote Sens. Environ. 118, 116–126.

O'Reilly, J.E., Maritorena, S., Mitchell, B.G., Siegel, D.A., Carder, K.L., Garver, S.A., Kahru, M., McClain, C., 1998. Ocean color chlorophyll algorithms for SeaWiFS. J. Geophys. Res. Oceans 103, 24937–24953.

Qi, L., Hu, C., Duan, H., Barnes, B.B., Ma, R., 2014. An EOF-based algorithm to estimate chlorophyll a concentrations in Taihu Lake from MODIS land-band measurements: implications for near real-time applications and forecasting models. Remote Sens. 6, 10694–10715.

Qian, X., Liu, L., Chen, X., Zhang, X., Chen, S., Sun, Q., 2022. The global leaf chlorophyll content dataset over 2003–2012 and 2018–2020 derived from MERIS/OLCI satellite data (GLCC): algorithm and validation. Earth Syst. Sci. Data Discuss. 1–21.

Qin, Z., Ruan, B., Yang, J., Wei, Z., Song, W., Sun, Q., 2022. Long-term dynamics of chlorophyll-a concentration and its response to human and natural factors in Lake Taihu based on MODIS data. Sustain 14, 16874.

Shi, W., Wang, M., 2007. Detection of turbid waters and absorbing aerosols for the MODIS Ocean color data processing. Remote Sens. Environ. 110, 149–161.

Shi, K., Zhang, Y., Zhu, G., Liu, X., Zhou, Y., Xu, H., Qin, B., Liu, G., Li, Y., 2015. Long-term remote monitoring of total suspended matter concentration in Lake Taihu using 250 m MODIS-aqua data. Remote Sens. Environ. 164, 43–56.

Simis, S.G.H., Liu, X., Cretaux, J.-F., Yesou, H., Malnes, E., Vickers, H., Blanco, P., Merchant, C.J., Carrea, L., Duguay, C., 2020. Product validation and algorithm selection report (PVASR) and algorithm development plan (ADP), pp. 23–26.

Simis, S., Liu, X., Calmettes, B., Yésou, H., Merchant, C., Carrea, L., Duguay, C., Wu, Y., 2022. Product Validation and Intercomparison Report (PVIR V2.1), pp. 149–152.

Soppa, M.A., Silva, B., Steinmetz, F., Keith, D., Scheffler, D., Bohn, N., Bracher, A., 2021. Assessment of polymer atmospheric correction algorithm for hyperspectral remote sensing imagery over coastal waters. Sensors 21, 4125.

Spyrakos, E., O'Donnell, R., Hunter, P.D., Miller, C., Scott, M., Simis, S.G., Neil, C., Barbosa, C.C., Binding, C.E., Bradt, S., 2018. Optical types of inland and coastal waters. Limnol. Oceanogr. 63, 846–870.
Steinmetz, F., Deschamps, P.Y., Ramon, D., 2011. Atmospheric correction in presence of sun glint: application to MERIS. Opt. Express 19, 9783–9800.
Tibshirani, R., Walther, G., Hastie, T., 2001. Estimating the number of clusters in a data set via the gap statistic. J. R. Stat. Soc. B 63, 411–423.
Tilstone, G.H., Lotliker, A.A., Miller, P.I., Ashraf, P.M., Kumar, T.S., Suresh, T., Ragavan, B., Menon, H.B., 2013. Assessment of MODIS-Aqua chlorophyll-a algorithms in coastal and shelf waters of the eastern Arabian Sea. Cont. Shelf Res. 65, 14–26.
Tilstone, G., Mallor-Hoya, S., Gohin, F., Couto, A.B., Sá, C., Goela, P., Cristina, S., Airs, R., Icely, J., Zühlke, M., 2017. Which ocean colour algorithm for MERIS in North West European waters? Remote Sens. Environ. 189, 132–151.
Wang, M., Son, S., Shi, W., 2009. Evaluation of MODIS SWIR and NIR-SWIR atmospheric correction algorithms using SeaBASS data. Remote Sens. Environ. 113, 635–644.
Wang, D., Ronghua, M., Xue, K., Li, J., 2019. Improved atmospheric correction algorithm for Landsat 8–OLI data in turbid waters: a case study for the Lake Taihu, China. Opt. Express 27, A1400–A1418.
Warren, M.A., Simis, S.G.H., Martinez-Vicente, V., Poser, K., Bresciani, M., Alikas, K., Spyrakos, E., Giardino, C., Ansper, A., 2019. Assessment of atmospheric correction algorithms for the sentinel-2A MultiSpectral imager over coastal and inland waters. Remote Sens. Environ. 225, 267–289.
Wynne, T.T., Mishra, S., Meredith, A., Litaker, R.W., Stumpf, R.P., 2021. Intercalibration of MERIS, MODIS, and OLCI satellite imagers for construction of past, present, and future cyanobacterial biomass time series. Remote Sens. 13, 2305.
Zeng, C., Binding, C.E., 2021. Consistent multi-mission measures of inland water algal bloom spatial extent using MERIS, MODIS and OLCI. Remote Sens. 13, 3349.
Zhang, Y., Ma, R., Duan, H., Loiselle, S., Zhang, M., Xu, J., 2016. A novel MODIS algorithm to estimate chlorophyll a concentration in eutrophic turbid lakes. Ecol. Indic. 69, 138–151.
Zhang, M., Hu, C., Cannizzaro, J., English, D., Barnes, B.B., Carlson, P., Yarbro, L., 2018. Comparison of two atmospheric correction approaches applied to MODIS measurements over North American waters. Remote Sens. Environ. 216, 442–455.
Zhao, M., Bai, Y., Li, H., He, X., Gong, F., Li, T., 2022. Fluorescence line height extraction algorithm for the geostationary ocean color imager. Remote Sens. 14, 2511.